Luo *et al. Carbon Research* (2023) 2:14
https://doi.org/10.1007/s44246-023-00045-5

Carbon Research

REVIEW

Open Access

g-C_3N_4-based photocatalysts for organic pollutant removal: a critical review

Yidan Luo[1], Yaowei Zhu[1], Yu Han[1], Huiyin Ye[1], Ruochen Liu[1], Yuanwang Lan[1], Mingshan Xue[1*], Xianchuan Xie[2], Shuohan Yu[3], Longshuai Zhang[4], Zuozhu Yin[1] and Bin Gao[5*]

Abstract

With rapid global industrialization, environmental pollution has become one of the major problems of human society. Photocatalysis can be applied to solve environmental problem by using inexhaustible solar energy. As a novel two-dimensional material, graphite carbon nitride (g-C_3N_4) has been widely applied in many photocatalytic reactions. However, in terms of its practical applications, g-C_3N_4 still has limitations, including poor photoexcited charge separation, limited range of visible light absorption, and low surface areas. Hence, current research on g-C_3N_4 mainly focuses on improving its photocatalytic performance. In this review, we summarize various methods to improve g-C_3N_4's light absorption and photo-induced charge transfer, including vacancy engineering, morphology control, heteroatom doping, and forming heterostructure. The applications of g-C_3N_4 and its derivatives in photodegradation of organic pollutants are also discussed in detail. Finally, the challenges and future research directions of g-C_3N_4 photocatalysts are summarized to promote their environmental applications.

Highlights

- Structural and optical properties of g-C_3N_4 are summarized in detail.
- Methods for improving the photocatalytic activity of g-C_3N_4 are reviewed.
- Applications of g-C_3N_4 in organic pollutant removal are discussed in detail.
- Challenges and future direction of g-C_3N_4 for degrading organic pollutants are summarized.

Keywords Heterostructure, Graphitic carbon nitride, Photocatalysis, Photodegradation, Water treatment

Handling editor: Baoshan Xing.

*Correspondence:
Mingshan Xue
xuems04@mails.ucas.ac.cn
Bin Gao
bg55@ufl.edu
Full list of author information is available at the end of the article

Springer

© The Author(s) 2023. **Open Access** This article is licensed under a Creative Commons Attribution 4.0 International License, which permits use, sharing, adaptation, distribution and reproduction in any medium or format, as long as you give appropriate credit to the original author(s) and the source, provide a link to the Creative Commons licence, and indicate if changes were made. The images or other third party material in this article are included in the article's Creative Commons licence, unless indicated otherwise in a credit line to the material. If material is not included in the article's Creative Commons licence and your intended use is not permitted by statutory regulation or exceeds the permitted use, you will need to obtain permission directly from the copyright holder. To view a copy of this licence, visit http://creativecommons.org/licenses/by/4.0/.

Graphical Abstract

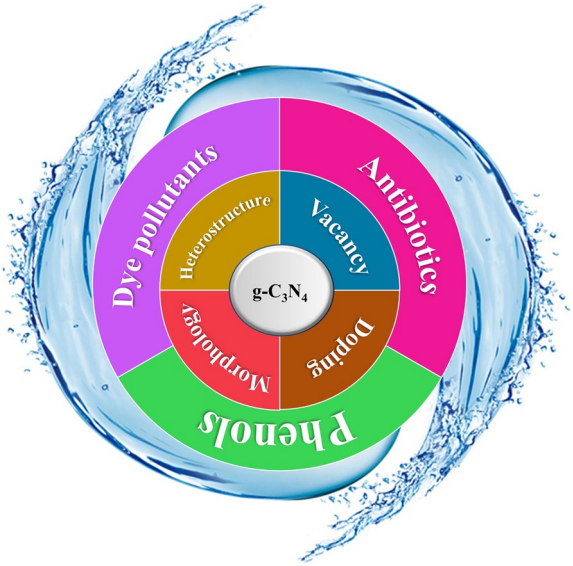

1 Introduction

In recent decades, numerous wastewater pollutants such as dyes, phenols, and antibiotics have inevitably been released into the soil, water, rivers, and lakes, which have a negative effect on human health and ecosystem (Qiu et al. 2021). Many water treatment technologies including precipitation, biodegradation, filtration, advanced oxidation, adsorption, and photocatalysis are widely used to remove pollutants from water (Lu et al. 2022b). Among them, photocatalysis has significant applications in water purification due to its low cost, environmental friendliness, and strong removal ability.

In 1972, Fujishima and Honda found that under light irradiation, water can be decomposed into O_2 and H_2 in an electrochemical cell (Fujishima and Honda 1972). Since then, photocatalysis has been widely reported. Extensive research about the applications of heterostructure photocatalysis has been carried out, such as water treatment, water splitting, volatile organic compound (VOC) removal, and CO_2 reduction to fuels (Liu et al. 2022; Zhang et al. 2022b). Photocatalysis happens when semiconductors absorb the energy of photons to generate electron–hole pairs, and then they quickly separate electron–hole pairs to produce active radicals for redox reactions such as degradation of organic pollutants (Lu et al. 2022a; Luo et al. 2022c). As a novel C and N based two-dimensional material, graphitic carbon nitride (g-C_3N_4) is regarded as a new generation of photocatalyst and has been widely used in the field of environmental photocatalysis.

Recent research trend on g-C_3N_4 photocatalyst from the "Web of Science" database is displayed in Fig. 1. The search was conducted using the keywords "g-C_3N_4" and "photocatalysis", which generated a total of 5462 articles in 2009–2021. When "water" was added as another keyword, the number of searched articles was 3130. The results were classified by year. We can see that g-C_3N_4 has been receiving increased attention for water treatment in the past decade. Fewer than five articles were published before 2011, and then the number increased significantly from 2012, and reached 771 articles in 2021.

Figure 2 shows the global distribution of papers about the g-C_3N_4-based systems for the removal of dyes, antibiotics, and phenols. The number of papers from different countries and their spatial distribution can be visualized. The number of papers is revealed using point distribution, where a point equals 20 papers. It is possible that some papers were double-counted because there were cases of co-authorship by authors from different countries. These countries were mainly distributed in Asia and Europe. In Asia, countries like China, India, Iran, Pakistan, South Korea, and Japan had many papers. The papers from Europe were mainly distributed among France, Spain, and Germany. In addition, the United States and Australia also published a considerable

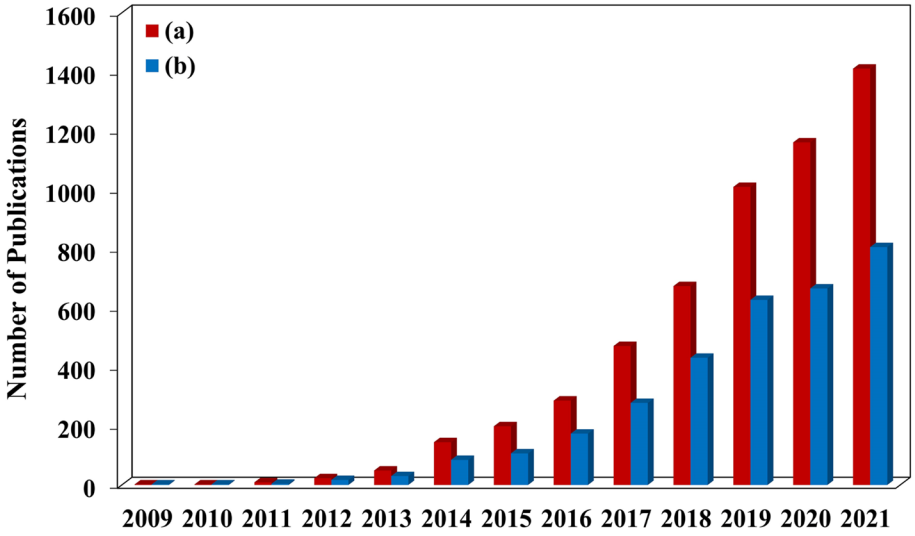

Fig. 1 **a** Number of annual publications using "g-C_3N_4" and "photocatalyst" as keywords; **b** Number of annual publications using "g-C_3N_4", "photocatalyst", and "water" as keywords. (Obtained from the "Web of Science")

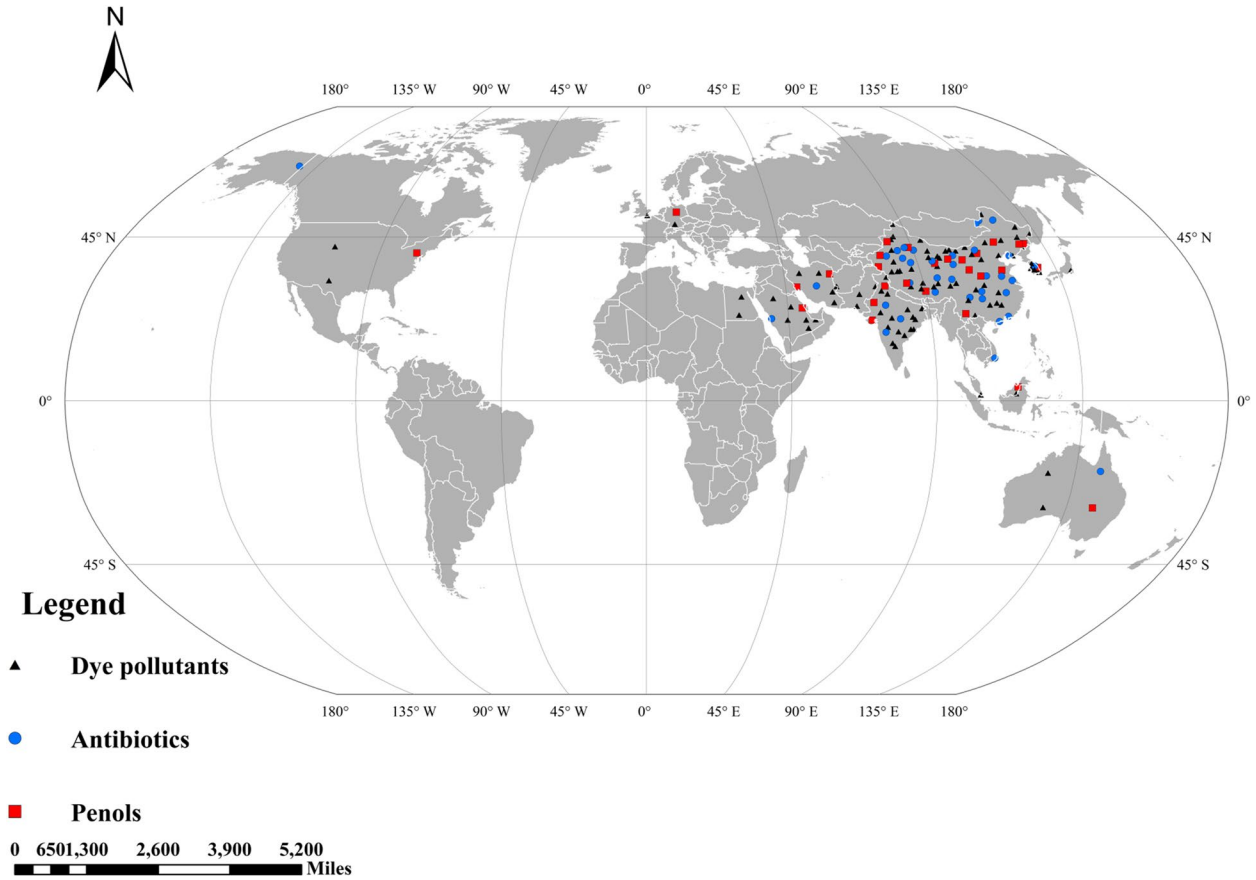

Fig. 2 The global distribution of the number of papers on g-C_3N_4-based photocatalysts for the removal of dyes, antibiotics, and phenols

number of papers. It is easy to see that g-C_3N_4-based photocatalyst is a hot research topic worldwide.

Nitrogen-rich precursors including urea, thiourea, dicyandiamide, melamine, etc. are usually used for the synthesis of g-C_3N_4 by the thermal polymerization method (Ong et al. 2016). The morphology of g-C_3N_4 is similar to graphite which shows a two-dimensional layered microstructure. The tri-s-triazine structure of g-C_3N_4 is the most stable phase (Zheng et al. 2015), which is regarded as the typical formation of g-C_3N_4. The π-conjugated structure of g-C_3N_4 is sp^2-hybridized by carbon and nitrogen. The ideal C/N molar ratio of g-C_3N_4 is 0.75, but most reported g-C_3N_4 is rich with defects, and the C/N molar ratio is close to 0.75, which makes it more activated in catalysis. The elements C and N are earth-abundant, resulting in low-cost preparation. A small amount of hydrogen of amine groups existed in g-C_3N_4. The surface defects and hydrogen are important in photocatalysis, which can serve as surface active sites for reactants adsorption and photocatalysis (Luo et al. 2023). The bandgap of g-C_3N_4 is around 2.7 eV with the conduction band (CB) and valence band (VB) potentials at ca. -1.1 eV and 1.6 eV, respectively, resulting in the visible light driven photodegradation.

However, pristine g-C_3N_4 has some disadvantages, including a narrow visible-light response range, small surface areas, and a low separation rate of electron–hole pairs. All these adverse factors significantly reduce photocatalytic efficiency (Tan et al. 2021). To enhance the applications of g-C_3N_4 in photocatalysis, various ways have been developed to improve its abilities for light adsorption and transfer of electron–hole pairs, including morphology control, the introduction of defects, doping with other atoms, coupling with metal, semiconductor, and carbonaceous materials (Fig. 3). To date, there are many photocatalytic applications of g-C_3N_4 in wastewater treatment, including removal of dyes, antibiotics, phenols, etc. This review mainly focuses on: (1) summarizing recent development of design and preparation of g-C_3N_4-based photocatalysts, (2) systematically reviewing the photocatalytic mechanisms on different water pollutants, (3) outlining future challenges and prospects of g-C_3N_4-based photocatalysts for pollutant degradation.

2 g-C_3N_4-based photocatalysts

Many methods have been developed to prepare g-C_3N_4. Among them, the thermal polymerization method is the most common method. In general, g-C_3N_4 is easily synthesized by thermal polymerization of nitrogen-rich precursors including urea (Li et al. 2021b), melamine (Xu et al. 2020a), dicyandiamide (Bai et al. 2014), cyanamide (Liu et al. 2014b), and thiourea (Dong et al. 2013) at different temperatures. Figure 4 shows the temperature and atmosphere for preparing g-C_3N_4 from different precursors.

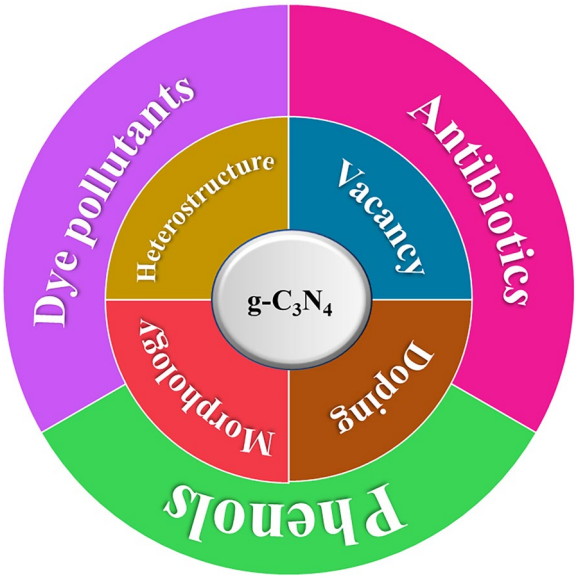

Fig. 3 Modification methods and applications of g-C_3N_4-based photocatalysts

2.1 Vacancy engineering

To improve the photocatalytic efficiency of g-C_3N_4, vacancy engineering is an effective way. g-C_3N_4 with nitrogen deficiency was successfully prepared by thermal treatment of the mixture of Melamine and NaOH (Luo et al. 2021). After heating with NaOH, the N/C atomic ratio was slightly reduced according to the organic elemental analyzer and X-ray photoelectron spectroscopy (XPS) results. The existence of nitrogen vacancies in g-C_3N_4 served as centers for oxidation, reduction, and charge recombination, which promoted the generation of h^+, $\bullet O_2^-$, and $^1O_2$, thus generating H_2O_2 in five different ways. According to the research of Wang et al. (2021a), N vacancy modification on g-C_3N_4 nanotube can promote the activation of peroxymonosulfate (PMS) with visible-light irradiation, and perform well in real water background and a wide pH range. N vacancy in g-C_3N_4 nanotube enhanced PMS adsorption and reduced it into •OH, which was the major oxidant. The C atoms near N vacancy showed electron-deficient and promoted the generation of $\bullet O_2^-$. Liang et al. (2018) reported C vacancies in g-C_3N_4 promoted the photocatalytic removal ability of Bisphenol A (BPA). C vacancies in g-C_3N_4 trapped photoinduced electrons and diminished the recombination of photoinduced carriers. The trapped photogenerated electrons in carbon vacancies transferred to O_2 to form $\bullet O_2^-$, which improved the BPA removal efficiency. According to Gao's research (2021), the CB of g-C_3N_4

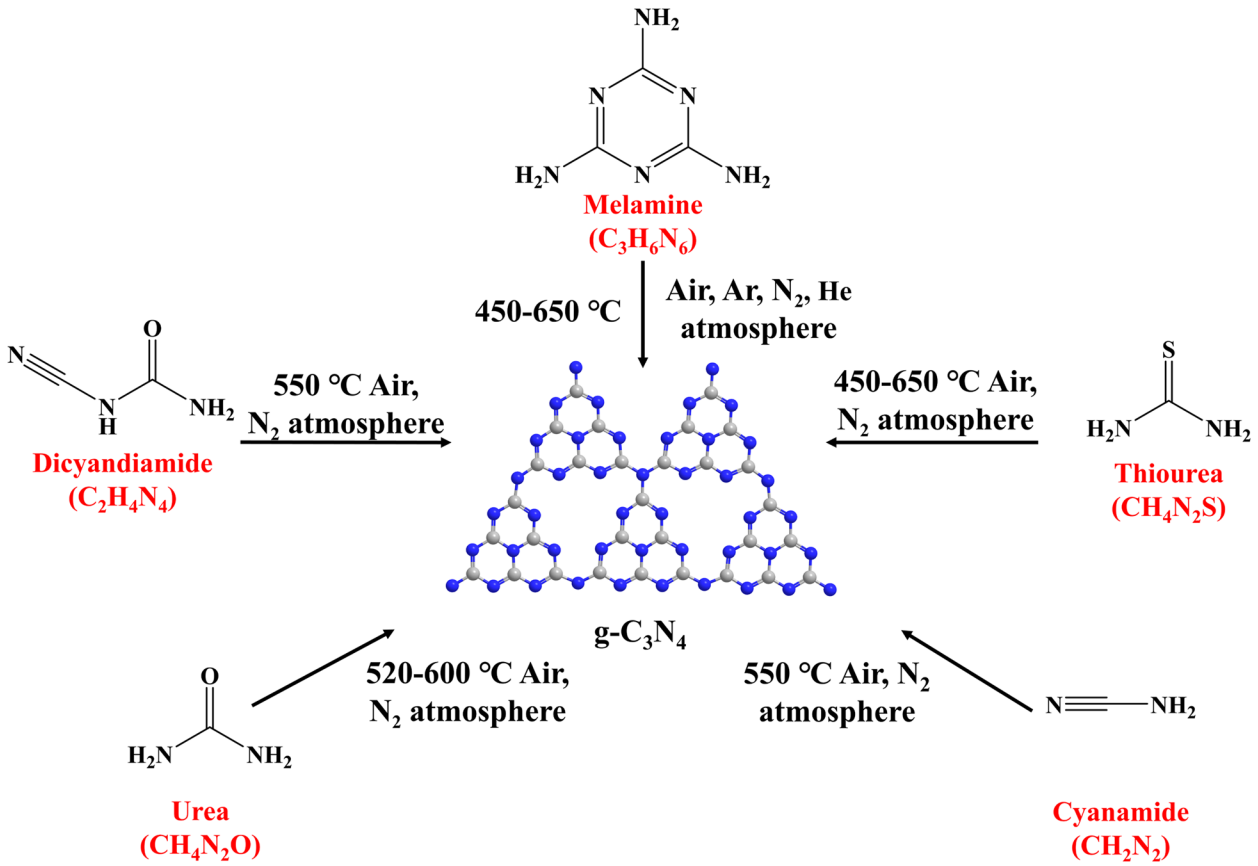

Fig. 4 Preparation of g-C_3N_4 from different precursors (Sudhaik et al. 2018; Abu-Sari et al. 2022; Nguyen et al. 2022)

moved to higher energy due to the C vacancy. The C vacancy modified g-C_3N_4 showed 57 folders of hydrogen production efficiency and higher degradation efficiency for many pollutants such as rhodamine B (RhB), tetracycline (TC), norfloxacin (NOR), ciprofloxacin (CPX), and levofloxacin.

Based on the above results, we can conclude that C and N vacancies in g-C_3N_4 may serve as active sites for the reactant's adsorption, promote the separation of photo-induced carriers, and change the band structure, which enhance the photocatalytic removal ability of many pollutants.

2.2 Morphology control

Morphology engineering of g-C_3N_4 is a vital area of current research. Many interesting morphologies of g-C_3N_4 have been successfully synthesized, including nanosphere, nanotube, nanosheet, and nanoflower. The g-C_3N_4 hollow nanospheres decorated with Pt were prepared by the thermal polymerization method with a silica template and cyanamide as the precursor (Benisti et al. 2021). In the O_2 generation, the maximal apparent quantum efficiency of g-C_3N_4 nanospheres was 12–15% and improved to 40–45% after loading with Pt. The g-C_3N_4 nanospheres were steady during 40 h of illumination. Liu et al. (2017) synthesized g-C_3N_4 nanorods with porous shells by thermal condensation of cyanamide in silica nanotube template and further etched by HF solution. The nanorods showed enhanced photocatalytic activity and good stability in water splitting and degradation of RhB.g-C_3N_4 can absorb the light with a wavelength of less than 475 nm (Li et al. 2020c). The bandgap will increase with the reduction of the number of nanosheets, resulting in a quantum confinement effect. Many methods were reported to diminish the thickness of the g-C_3N_4 sheets to a few atomic layers. Thermal oxidation can etch bulk g-C_3N_4 to 2 nm in thickness, according to the research of Niu et al. (Niu et al. 2012). The obtained anisotropic two dimensions (2D) g-C_3N_4 nanosheets have a higher specific surface area (306 m^2/g), larger bandgap, enhanced in-plane electron transfer ability, and increased photo-induced carriers' lifetime. Acid or alkali stripping is also an effective method to separate the g-C_3N_4 layers into thin nanosheets (Taizo et al. 2013; Cui et al. 2018). The g-C_3N_4 exfoliated by H_2SO_4 and HNO_3 extended the bandgap and drastically prolonged the recombination

of photo-induced carriers (Leong et al. 2018), and it showed improved photoactivity in the removal of BPA under direct sunlight. Compared with bulk g-C_3N_4, the alkali-etched g-C_3N_4 exhibited thinner and more porous g-C_3N_4 nanosheets with larger specific surface area (Feng et al. 2017a), more exposed active sites, shorter carrier diffusion length, faster efficiencies of RhB degradation and hydrogen production. Mechanical strategies including ultrasonic stripping and ball milling were applied to decrease the particle size and stacked layers in g-C_3N_4 nanosheets. The photodegradation of RhB on atomic single layer g-C_3N_4 prepared by the ultrasonic exfoliating process was 10.2 times and 3.0 higher than that on the g-C_3N_4 nanosheets with bulk morphology and few layers (Zhao et al. 2013). Ultrathin and easily dispersed g-C_3N_4 nanosheets prepared by wet ball milling exhibited 2.2 times photocatalytic activity of RhB compared to untreated g-C_3N_4 nanosheets (Ma et al. 2021b).

The morphology engineering of g-C_3N_4 is an effective way to obtain specific properties. For example, one-dimensional (1D) rod structure can effectively improve the separation efficiency of photogenerated carriers. Two-dimensional (2D) structure usually creates large specific surface area for more active adsorption sites for photocatalytic degradation. Three-dimensional (3D) structure makes g-C_3N_4 have great application potential in the field of photodegradation due to the advantages of stable photocatalytic performance and easy-recycling ability. The information is expected to provide insights into the subsequent design of g-C_3N_4-based systems with specific properties.

2.3 Heteroatom doping

Element doping can not only adjust the energy band structure of g-C_3N_4 by adjusting the VB and CB, but also affect the surface properties of the photocatalyst, thereby improving its photocatalytic performance (Xing et al. 2022). By introducing non-metallic elements with different electronegativity and atomic radius from C and N elements, the charge redistribution of g-C_3N_4 will be changed, which may lead to a change of the photocatalytic effect. Moreover, the introduction of non-metallic elements can increase the delocalization of π-conjugated electrons, resulting in a decrease in the band gap to improve the utilization of visible light (Tang et al. 2023). The introduction of metal impurities can produce additional binding effects and form a metal-Nx active site, enhancing the charge transfer capacity of the photocatalyst, reducing its band gap, and enhancing its adsorption capacity, thereby improving the photocatalytic activity (Xing et al. 2022).

Metal or non-metal atoms doped g-C_3N_4 can be easily prepared to improve their light absorbance and tune band energies for photocatalytic reactions. Doping many non-metallic elements like B, O, F, P, S, Cl, Br, and I was reported as an effective method to promote photocatalytic efficiency (Luo et al. 2016; Feng et al. 2019; Liu et al. 2019; Mian et al. 2020; Hu et al. 2020). The O doped g-C_3N_4 was obtained with double oxidation of the concentrated acid-ultrasound method (Yang and Bian 2021). The sufficient oxygen-containing functional groups and pit-like defects were formed on the surface of g-C_3N_4 by an appropriate degree of oxidation, thereby enhancing photocatalytic performance. The oxygen doping changed the main active species of g-C_3N_4 in the photodegradation of RhB from h^+ to $^1O_2$. The photocatalytic degradation efficiency of C and O doped g-C_3N_4 for indomethacin was 5.9 times higher than bulk g-C_3N_4, and the main reactive species were $^1O_2$ and $\bullet O_2^-$ (Zheng et al. 2020). The P, O co-doped g-C_3N_4 was successfully synthesized by a facile thermal polymerization method, and its degradation rate for enrofloxacin was 6.2 times higher than that of g-C_3N_4 (Huang et al. 2019). Based on the nuclear magnetic resonance spectroscopy and XPS, some carbon sites were replaced by P atoms, and the nitrogen sites in the framework of g-C_3N_4 were replaced by O atoms. The improved photocatalytic degradation of enrofloxacin was attributed to the enhanced surface area, narrow bandgap, and effective charge separation, and $\bullet O_2^-$ was the main active species. The S and Cl co-doped g-C_3N_4 nanosheets have a narrower band gap and better carriers' separation ability (Yi et al. 2020), which may be ascribed to the doping level of Cl 3p orbital according to the first-principles calculations. The S and Cl co-doping positively shifted the VB potential of CN and improved the photocatalytic activities for the degradation of 4-nitrophenol (4-NP) and RhB. In the P, S, and O-co-doped g-C_3N_4 hydrogel, the C and N atoms were replaced and C-S, C-O, and P-N bonds were formed (Chu et al. 2020). The P, S, and O doping facilitated charge separation across the heptazine rings and attracted photoexcited electrons, which exhibited enhanced photocatalytic activity for methylene blue (MB) removal.

Doping with metal atoms has been widely investigated to enhance the photoactivity of g-C_3N_4. Er-doped g-C_3N_4 were synthesized by thermal condensation of $Er(NO_3)_3{\cdot}5H_2O$ and melamine for photodegradation of tylosin, RhB, and TC (Li et al. 2020a). The Er doping narrowed the bandgap and increased the photocatalytic activity. The leaching toxicity of Er-doped g-C_3N_4 could be ignored. The Ce-doped mesoporous g-C_3N_4 photocatalyst was constructed by plant growing guide and calcination method (Zhu et al. 2020). The improved degradation of 2-mercaptobenzothiazole was ascribed to the biomass

carbon enhancing the mass transport channels of carriers. The doped Ce^{4+} ions served as the redox center can degrade pollutants with photo-induced carriers.

Doping metal/nonmetal atoms to improve the performance of g-C_3N_4 is a simple way to improve its photocatalytic performance. This strategy can reduce the band gap of the semiconductor to improve its optical properties and charge transfer performance. Therefore, photocatalytic abilities of metal/nonmetal atom-doped g-C_3N_4 are improved and their applications in wastewater treatment are broadened.

2.4 Heterostructure

Constructing heterostructure is another effective method to increase light absorption and enhance the photogenerated charge separation and transfer. The construction of heterojunction photocatalyst should satisfy the requirement that the coupling semiconductors have an appropriate electronic band structure to form band arrangement. As shown in Fig. 5, the heterojunctions are classified as type I, type II, Schottky junction, and Z-scheme, which provide different charge transfer processes (Hou and Zhang 2020; Luo et al. 2022b). In the Type I heterostructure (Fig. 5a), the VB and CB of photocatalyst II (PII) are located within the band gap of photocatalyst I (PI), so electrons and holes are accumulated in photocatalyst II (PII) (Kumar et al. 2022). The type II heterostructure (Fig. 5b) could transfer electrons and holes to two different photocatalysts separately with staggered VB and CB (Yuan et al. 2021b). In the Schottky junction (Fig. 5c) (Fauzi et al. 2022), driven by the Fermi level potential difference between the two materials, photoelectrons can flow from semiconductor to cocatalyst through the interface. Therefore, the formed Schottky junction can be used as an electron trap to effectively attract photoinduced electrons, resulting in effective photoinduced charge separation. Z-scheme and type II heterojunction have similar band structures, but

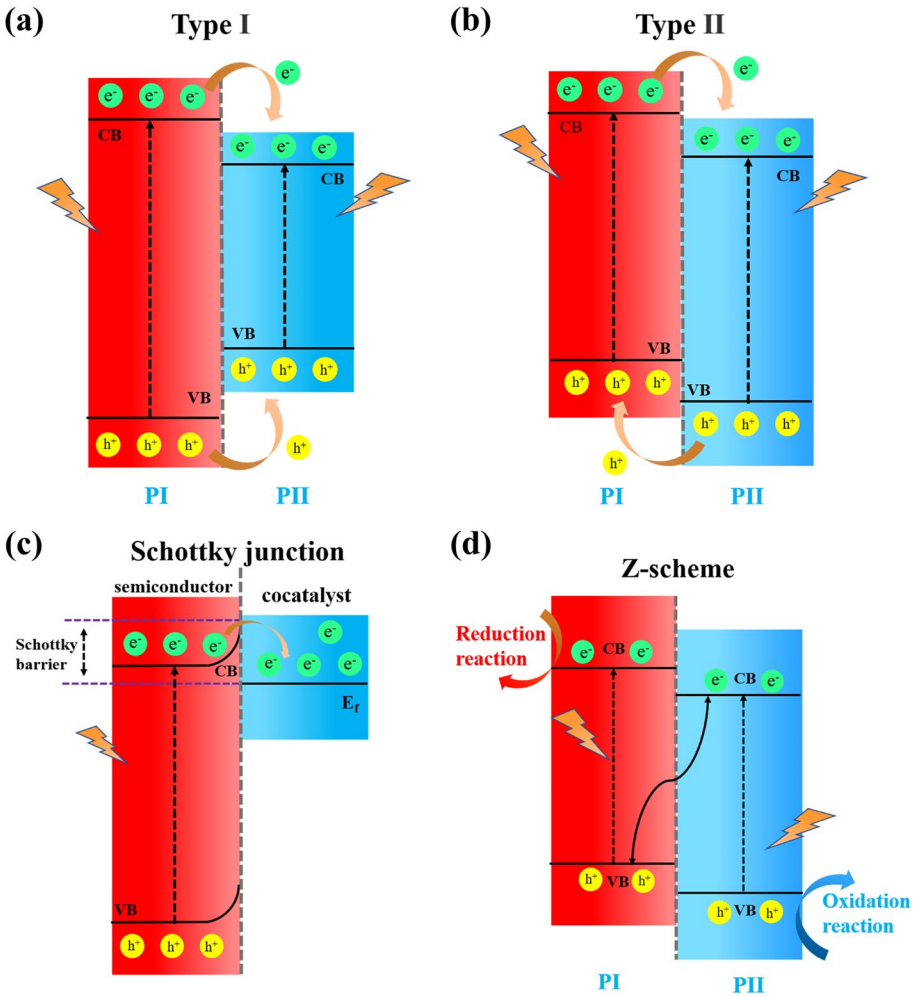

Fig. 5 Schematic diagrams of four types of heterojunctions (Prabavathi et al. 2019; Hou and Zhang 2020; Jiang et al. 2020; Xu et al. 2020b)

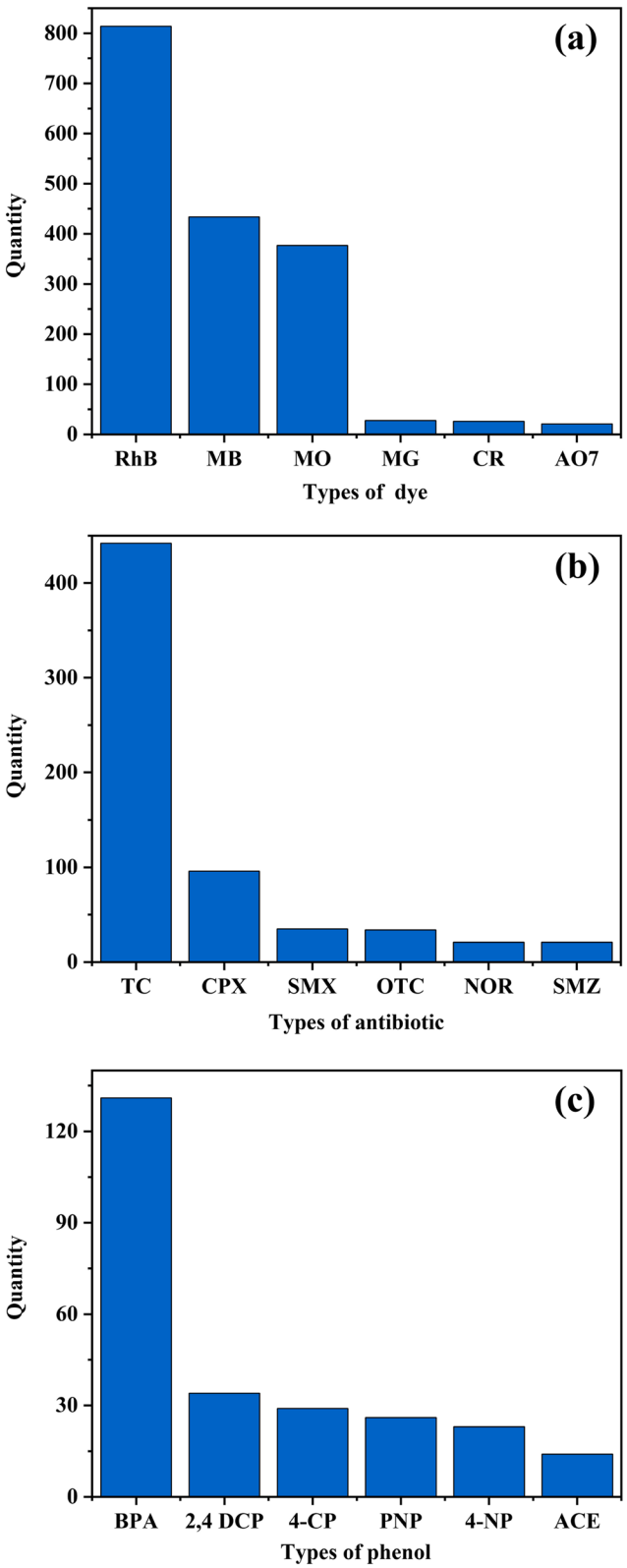

Fig. 6 Number of papers of g-C_3N_4-based photocatalysts in the removal of dye pollutants (**a**), antibiotics (**b**), and phenols (**c**)

Table 1 Chemical structures of various organic pollutants

Pollutants	Structure	Ref
Rhodamine (RhB)	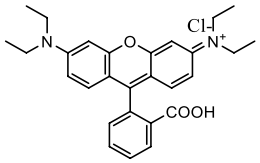	(Jaleh et al. 2021)
Methylene blue (MB)	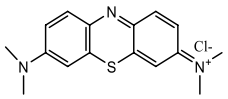	(Song et al. 2019)
Methyl orange (MO)	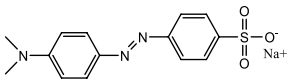	(Jaleh et al. 2021)
Malachite green (MG)	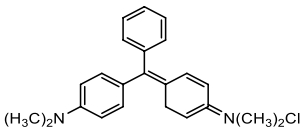	(Lin et al. 2018)
Congo red (CR)	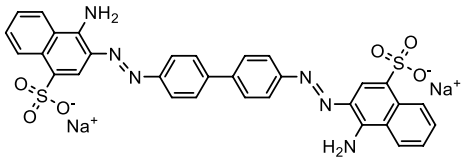	(Jaleh et al. 2021)
Acid orange 7 (AO7)	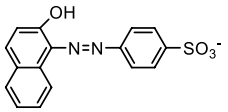	(Wang et al. 2021d)
Tetracycline (TC)	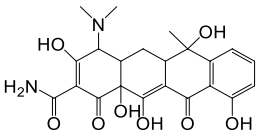	(Zhang et al. 2021b)
Ciprofloxacin (CPX)	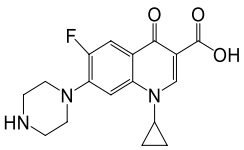	(Raja et al. 2020)
Sulfamethoxazole (SMX)	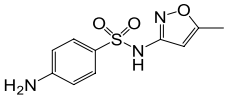	(Kutuzova et al. 2021)
Oxytetracycline (OTC)	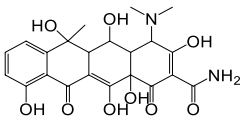	(Ye et al. 2019)
Norfloxacin (NOR)	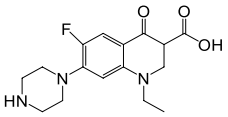	(Tian et al. 2018)
Sulfamethazine (SMZ)	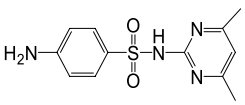	(Zhang et al. 2021a)

Table 1 (continued)

Pollutants	Structure	Ref
Bisphenol A (BPA)	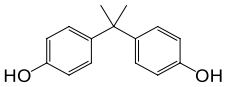	(Jaleh et al. 2021)
2,4-dichlorophenol (2,4-DCP)	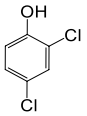	(Qu et al. 2020)
4-chlorophenol (4-CP)	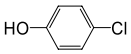	(Jaleh et al. 2021)
P-nitrophenol (PNP)	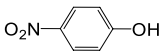	(Darie et al. 2019)
4-nitrophenol (4-NP)	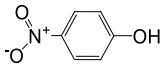	(Jaleh et al. 2021)
Acetaminophen (ACE)	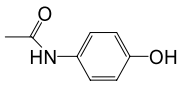	(Mu et al. 2020)

the direction of electron transfer is different. As shown in Fig. 5d (Xu et al. 2018), the electrons in CB of PII will recombine with holes in VB of PI, and holes with strong oxidation ability in PII and electrons in the CB of PI with strong reduction abilities are preserved, resulting in enhanced photocatalytic activity.

Choosing two or more semiconductor materials to construct heterojunction structure reasonably can integrate the advantages of many effects to improve the separation of photogenerated charges, expand the absorption range of visible light, and maintain the high redox ability of photocatalyst. Therefore, the design and synthesis of different types of g-C_3N_4-based heterojunction photocatalysts can effectively improve photocatalytic performance and are widely used in the field of environmental water treatment.

3 Photocatalytic degradation of organic pollutants

Recently, the photocatalytic applications of g-C_3N_4-based materials in the environment have attracted wide attention. In this part, the photodegradation applications of g-C_3N_4-based materials for dye pollutants, antibiotics, and phenols are reviewed. Figure 6 shows the number of publications on the removal of various dye pollutants, antibiotics, and phenols.

The structures of these pollutants are presented in Table 1. Dyes are an important pollutant, which can even be identified by naked eyes. Usually, dyes pollute the water bodies and cause skin allergy and eye irritation. Therefore, it is necessary to eliminate dye pollution in the environment. According to their chemical structure, dyes are mainly divided into azo dyes, anthraquinone dyes, xanthene dyes, triarylmethane dyes, thiazine dyes, etc. Azo dyes such as acid orange 7 (AO7), congo red (CR), and methyl orange (MO) are cost-effective and stable (Rauf and Ashraf 2009; Raval et al. 2016). Compared with azo dyes, anthraquinone dyes such as pigment yellow 108 are less stable and more expensive (Gupta and Suhas 2009). The xanthene dyes such as RhB usually exhibit yellow, pink or red color depending on the functional group. Triarylmethane dyes such as malachite green (MG) are synthetic organic compounds with three aryl groups connected to the central carbon atom (Rauf and Ashraf 2009). Thiazine dyes such as MB are mostly used dyes for laboratory uses (Kiernan and Histochemistry 2001; Le et al. 2022). According to their chemical structures, antibiotics can be divided into β-lactams, aminoglycosides, macrolides, amide alcohols, tetracyclines, polypeptides, lincosamides, polyphosphates, fluroquinolones, sulfonamides and so on (Pi et al. 2018; Biswal and Balasubramanian 2022). TC and oxytetracycline (OTC) are the most studied tetracyclines. CPX and NOR are the most concerned fluoroquinolones. In sulfonamides, sulfamethoxazole (SMX) and sulfamethazine (SMZ) have been widely studied (Margolis et al. 2010; Roca Jalil et al. 2015; Oliveira et al. 2019; Chandra et al. 2021; Shurbaji et al. 2021). Antibiotics may affect the distribution of microbial communities in water and affect humans through food chain transmission. At the same time, the prevalence of antibiotics may lead to antibiotic resistance (Qin et al. 2021). Phenolic compounds have at least one aromatic ring with one or more hydroxyl groups. Common phenols are BPA, 2,4-dichlorophenol (2,4-DCP), 4-chlorophenol (4-CP),

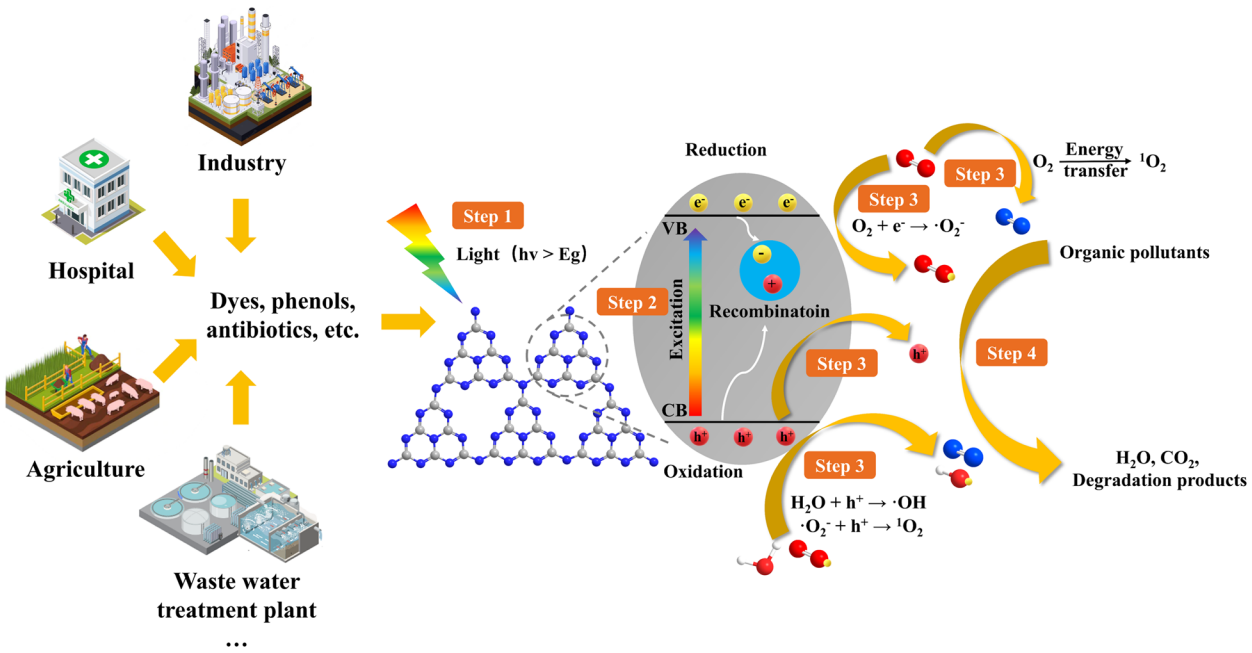

Fig. 7 Degradation mechanisms of g-C_3N_4 for organic pollutants of different sources (Song et al. 2017; Amanulla et al. 2018; Wei et al. 2021; Zhao et al. 2021b)

p-nitrophenol (PNP), 4-NP, acetaminophen (ACE) and so on. They are toxic and carcinogenic to humans, animals, and wildlife even at low concentrations (Liu et al. 2014a). Photocatalysis as an economically feasible way for the removal of dyes, antibiotics, and phenolic pollutants has attracted widespread attention.

The sources of antibiotics, phenols, and dyes are shown in Fig. 7. So far, g-C_3N_4 has been widely used as an environmental photocatalyst, therefore its photocatalytic degradation mechanism for organic pollutants has been explored. The photocatalytic process can be divided into four stages (Fig. 7). Firstly, visible light is absorbed by g-C_3N_4 (Step 1). The light absorption stage is up to the surface morphology and structure of the photocatalyst (Wen et al. 2017). When the energy of light is greater than or equal to the energy of the semiconductor band gap (E_g), the electrons are excited from VB to CB, leaving holes in VB, thus achieving effective separation of photogenerated carriers (Step 2) (Zhang et al. 2019). The band gap of g-C_3N_4 can be further adjusted by doping, introducing defects, etc. (Wen et al. 2017), thus promoting its use of visible light. At the same time, in order to promote photocatalysis, it is necessary to prevent the recombination of electrons and holes. Furthermore, photogenerated electrons and holes are separated and migrated (Step 3). Photogenerated electrons react with electron acceptors (such as oxygen) to form superoxide groups, and holes react with water to produce hydroxyl radicals (Ge et al. 2011). Singlet oxygen ($^1O_2$) can be produced by the reaction of holes with superoxide groups or reacting with oxygen by energy transfer (Zhang et al. 2009; Zhou et al. 2017). At last, g-C_3N_4 can adsorb the diffused pollutants on its surface, and the active substances degrade them into the water, carbon dioxide, and other products after redox reactions (Step 4). For each target pollutant, the photocatalytic mechanism will be different. The following sections summarize the degradation mechanisms for specific pollutants.

3.1 Degradation of dyes

Dyes pose a serious threat to the aqueous environment owing to their non-biodegradability and chemical stability in water. More than 100,000 organic dyes with an annual production of over 7×10^5 t are commercially available (Zhang et al. 2020b). Hence, green methods to treat dye pollutants with low-cost and high efficiency are urgently needed. g-C_3N_4-based materials have unique characteristics, such as tunable nanostructures, chemical stabilities, and rich active sites, making them particularly suitable for dye degradation (Liang et al. 2021). Table 2 lists the recent g-C_3N_4-based materials for dyes degradation in wastewater.

RhB is a water-soluble xanthene dye that irritates the eyes and skin and is deleterious if swallowed by animals and human beings (Liang et al. 2021). It is the most widely studied dye worldwide (Fig. 6a). The

Table 2 Information on the degradation of dye pollutants by g-C_3N_4-based photocatalyst[a]

Catalyst	Process conditions	Light source	Catalyst dosage	Performance	Active species	Ref
O-doped g-C_3N_4	RhB: 20 mg/L, 30 mL	350 W Xe lamp	30 mg	180 min, 100%	**$^1O_2$**, $\cdot O_2^-$, h^+	(Yang and Bian 2021)
Co_3O_4@g-C_3N_4	RhB: 20 mg/L, 50 mL	300 W Xe lamp	10 mg	60 min, 95%	$\cdot O_2^-$, h^+, •OH	(Rabani et al. 2021)
Ag-B doped g-C_3N_4	RhB: 10 mg/L, 50 mL	150 W Xe lamp	10 mg	80 min, 100%	**•OH**, $\cdot O_2^-$	(Roselin et al. 2019)
P-K doped g-C_3N_4	RhB: 20 mg/L, 100 mL	300 W Xe lamp ($\lambda \geq 420$ nm)	20 mg	80 min, 98.2%	**h^+**, $\cdot O_2^-$, •OH	(Shen et al. 2020)
g-C_3N_4/carbon nanotubes	RhB: 10 mg/L, 100 mL	300 W Xe lamp ($\lambda > 420$ nm)	20 mg	60 min, 98.1%	**$\cdot O_2^-$**, e^-, •OH	(Liu et al. 2020)
$BaTiO_3$/Au/g-C_3N_4	RhB: 5 mg/L, 100 mL	300 W Xe lamp	20 mg	20 min, 100%	**h^+**, **•OH**, $\cdot O_2^-$	(Wu et al. 2020)
BiOBr/g-C_3N_4	RhB: 10 mg/L, 100 mL	100 W Xe lamp	20 mg	30 min, 95.23%	**$\cdot O_2^-$**, **h^+**, •OH	(Zhang et al. 2021c)
Carbonized poly(tannic acid)/g-C_3N_4	RhB: 10 mg/L, 30 mL	500 W Xe lamp ($\lambda \geq 420$ nm)	30 mg	80 min, 97%	$\cdot O_2^-$, **h^+**, •OH	(Yang et al. 2021)
Perylene diimide-g-C_3N_4/MIL	RhB: 100 mg/L, 30 mL	Xe lamp	3 mg	60 min, 98%	**$\cdot O_2^-$**, **h^+**, **•OH**	(Wang et al. 2021c)
$Cd_{0.5}Zn_{0.5}S$/g-C_3N_4	RhB: 4.79 mg/L, 50 mL	350 W Xe lamp ($\lambda > 420$ nm)	50 mg	90 min	$\cdot O_2^-$, h^+, •OH	(Qin et al. 2020)
Bi_2MoO_6/g-C_3N_4	RhB: 5 mg/L, 100 mL	300 W Xe lamp ($\lambda > 420$ nm)	5 mg	40 min, 95.4%	**h^+**, $\cdot O_2^-$, •OH	(Li et al. 2020b)
Li doped g-C_3N_4/Co_3O_4	RhB: 10 mg/L, 50 mL	300 W Xe lamp	50 mg	60 min, 98%	**h^+**, $\cdot O_2^-$, •OH	(Niu et al. 2022)
g-C_3N_4/BiOI	RhB: 20 mg/L, 50 mL	500 W Xe lamp ($\lambda > 420$ nm)	20 mg	120 min, 99%	**h^+**, $\cdot O_2^-$, •OH	(Hou et al. 2021)
g-C_3N_4/Fe_3O_4/RGO	RhB: 15 mg/L, 50 mL	400 W metal halide lamp ($\lambda > 400$ nm)	10 mg	75 min, 100%	$\cdot O_2^-$, **•OH**, h^+	(Luo et al. 2022a)
N-doped carbon quantum dots (CQDs)/g-C_3N_4	MB: 10 mg/L, 100 mL	18 W LED lamp	50 mg	180 min, 54.6%	**h^+**, •OH, $\cdot O_2^-$	(Seng et al. 2020)
g-C_3N_4/ZnO, Zr/g-C_3N_4	MB: 10 mg/L, 200 mL	350 W Xe lamp ($400 \leq \lambda < 800$ nm)	100 mg	180 min, 98.07%	**h^+**, $\cdot O_2^-$, •OH	(Guo et al. 2020)
Ni-ZnS/g-C_3N_4	MB: 10 mg/L, 220 mL	500 W tungsten halogen direct lamp ($\lambda \geq 400$ nm)	220 mg	40 min, 96%	$\cdot O_2^-$, **•OH**, h^+	(Danish and Muneer 2021)
S-doped g-C_3N_4/TiO_2	CR: 50 mg/L, 100 mL	300 W Xe lamp	20 mg	60 min, 96.2%	$\cdot O_2^-$, **•OH**, h^+	(Wang et al. 2021b)
g-C_3N_4/ZnSe	CR: 100 mg/L, 80 mL	300 W Xe lamp ($\lambda > 420$ nm)	10 mg	60 min, 95.69%	$\cdot O_2^-$, •OH, $^1O_2$	(Ehsan et al. 2020)
BiOI-BiOCl/g-C_3N_4	AO7: 10 mg/L, 100 mL	400 W halogen lamp	100 mg	140 min, 97.4%	**h^+**, $\cdot O_2^-$, •OH	(Aghdam et al. 2017)

[a] The main active species in each reference are shown boldly in the table

SiO_2/g-C_3N_4 (Si-CN) composite photocatalyst and surface hydroxylation modified SiO_2/g-C_3N_4 (Si-CN-HO) were prepared for RhB degradation (Sun et al. 2021a, b). Firstly, SiO_2 and melamine are ground separately with ethanol to obtain two mixed slurries. Secondly, the two mixed slurries were grounded together and calcined in a muffle furnace to prepare Si-CN composite photocatalyst. The prepared Si-CN composites were refluxed in H_2O_2 solution to realize the surface hydroxylation modification of Si-CN-HO. The photocatalytic efficiency of RhB by hydroxylated Si-CN was 20.9 times of that by CN under solar light irradiation. Scanning electron microscopy (SEM) and transmission electron microscope (TEM) analyses showed that combining SiO_2 and CN significantly suppressed the clustering of CN nanosheets, in which SiO_2 acted as a space barrier to CN. In addition, hydroxyl-modified Si-CN further decreased the agglomeration of CN nanosheets, which could be ascribed to the escape of oxygen during surface modification. The specific surface area of Si-CN was 1.8 times of that of CN. It could be concluded from UV–Vis absorption spectra that Si-CN had higher light absorption intensity, due to the improvement of dispersion. The optical absorption intensity of Si-CN-HO was even better than that of Si-CN, which increased with the modification temperature. This might be due to the strong oxidation of H_2O_2 that caused some defects on the surface of CN, thus forming impurity levels and

improving the optical absorption capacity. In addition, the capture experiments confirmed that $\bullet O_2^-$ is the main active group for the photocatalytic degradation of RhB. The reaction mechanism reveals the reason for the photocatalytic activity enhancement of Si-CN-HO samples. The electrons on the VB of CN were excited by light and transited to the CB in Si-CN-HO. The holes left in the VB migrated to the semiconductor surface and were trapped by hydroxyl groups. At the same time, the electrons were trapped by oxygen to form $\bullet O_2^-$, which further degraded RhB.

The surface hydroxylation treatment of Si-CN composite led to the dispersion of SiO_2 on CN by enhancing the combination of SiO_2 and CN, resulting in an obvious improvement in surface area. This facilitated the adsorption of pollutants by Si-CN-HO, thus promoting pollutant degradation. In addition, the optical absorption performance of Si-CN-HO was better than that of bulk CN due to the optical reflection effect from SiO_2 and surface defects created by surface hydroxylation treatment, which improved the optical utilization efficiency in photocatalytic reaction.

The formation of heterojunction is an effective strategy to improve photocatalytic activity. Mo, N co-doped $ZnIn_2S_4$/g-C_3N_4 material (M, N-ZIS/CN) was prepared by sol–gel method for photodegradation of MB (Ma et al. 2022). Firstly, g-C_3N_4 was obtained by calcination using a three-step procedure. Then, zinc acetate and indium chloride were added to 150 mL distilled water and stirred for 30 min before thioacetamide was added. The g-C_3N_4 dispersed in distilled water was then added drop by drop. The solution was heated and dried to form a gel. The dried gel was washed and vacuum dried to obtain $ZnIn_2S_4$/g-C_3N_4 material. M, N-ZIS/CN nanosheets were obtained by adding ammonium molybdate and N–N-dimethylformamide to the solution for the preparation of $ZnIn_2S_4$/g-C_3N_4, and the rest procedures were the same as the preparation method of $ZnIn_2S_4$/g-C_3N_4 material. SEM and TEM analyses showed that $ZnIn_2S_4$ was a thick nanoflower structure, g-C_3N_4 was thin nanosheets, and $ZnIn_2S_4$/g-C_3N_4 was thin nanosheets, but M, N-ZIS/CN was small and loose 2D nanoflower. These indicate that co-doping increased the specific surface area of the composite material, increased its active site, shortened the charge transfer path, and reduced the agglomeration of $ZnIn_2S_4$ particles. UV–Vis absorption spectra showed that M, N-ZIS/CN had a wide absorption range in ultraviolet and visible light. Photocatalytic tests showed that M, N-ZIS/CN could degrade 97% of MB in 120 min, which was 2.6 times that of $ZnIn_2S_4$. In the cycle test, M, N-ZIS/CN used for the third time could still degrade 95.2% of MB, indicating that M, N-ZIS/CN had strong photocatalytic degradation ability and stability. The radicals trapping experiment found that e^-, $\bullet O_2^-$ and h^+ were the main active species of degrading pollutants, and their degradation mechanism was as follows:

$$M,N-ZIS+h\nu \rightarrow M,N-ZIS(e^-)+M,N-ZIS(h^+)$$
$$CN+h\nu \rightarrow CN(e^-)+CN(h^+)$$
$$CN(e^-)+O_2 \rightarrow CN+\cdot O_2^-$$
$$\cdot O_2^-+OH^- \rightarrow \cdot OH$$
$$\cdot O_2^-+\cdot OH+M,N-ZIS(h^+)+MB \rightarrow Degradation\ products$$

The Z-scheme heterostructure of M, N-ZIS/CN was prepared by sol–gel method. The internal electric field formed by the material accelerated the migration of charges and promoted the redox reaction.

Designing ternary g-C_3N_4-based composite heterostructure to improve photocatalytic performance is also booming. AgI-Ag_2S impregnated g-C_3N_4 (AgI-Ag_2S@g-C_3N_4) composites were synthesized by hydrothermal and pyrolysis methods (Velmurugan et al. 2020). g-C_3N_4 was prepared by thermal polymerization of dicyandiamide. AgI-Ag_2S was prepared by wet chemical route. Finally, g-C_3N_4 was ultrasonically dispersed in a methanol solution, and then a certain amount of AgI-Ag_2S powder was added to the above solution and stirred and heated until the methanol was completely evaporated to obtain AgI-Ag_2S@g-C_3N_4 photocatalyst. Based on the nitrogen adsorption and desorption isotherms, the surface area of AgI-Ag_2S@g-C_3N_4 nanocomposites increased, owing to the fact that AgI-Ag_2S can prevent the agglomeration of g-C_3N_4, thereby improving the adsorption of dyes on the active surface of the catalyst and enhancing the interaction between the photocatalyst and the pollutants. In addition, the optical absorption properties of the samples were analyzed by UV–Vis diffuse reflectance spectroscopy. Compared with the g-C_3N_4, the band gap of AgI-Ag_2S@g-C_3N_4 was significantly reduced and the light response range was increased, beneficial to the separation of photogenerated electron holes. The photogenerated charge separation was further studied by photoluminescence spectroscopy (PL). On the one hand, AgI-Ag_2S@g-C_3N_4 had a lower PL intensity, indicating that there was a lower photogenerated charge recombination rate in the composite material. On the other hand, with the slight shift of the characteristic band of g-C_3N_4 in the Raman spectrum of AgI-Ag_2S@g-C_3N_4 nanocomposites, the signal of g-C_3N_4 was highly enhanced, indicating that AgI-Ag_2S had strong adsorption on the g-C_3N_4 surface by charge transfer resonance. With Evans Blue (EB) and congo red as target contaminants, AgI-Ag_2S@g-C_3N_4 achieved 98.4% of EB degradation in 50 min and 94.2% of CR degradation in 30 min. In order to clarify the reasons for the enhancement of photocatalytic activity, the researchers explored its photocatalytic mechanism. It was found that a double Z-scheme heterojunction of g-C_3N_4-Ag_2S

and Ag_2S-AgI was formed in AgI-Ag_2S@g-C_3N_4, which effectively inhibited the recombination of photogenerated carriers, so that more active substances were used for photocatalytic reactions. The specific photocatalytic degradation process of organic dyes on AgI-Ag_2S@g-C_3N_4 nanocomposites was as follows:

$$AgI - Ag_2S@g - C_3N_4 + h\upsilon \rightarrow e^- + h^+$$
$$e^- + h^+ + H_2O \rightarrow \cdot O_2^- + \cdot OH^-$$
$$\cdot O_2^- + \cdot OH^- + Organic\ dye \rightarrow CO_2 + H_2O$$

Besides, AgI-Ag_2S@g-C_3N_4 had excellent cycle stability after dye photodegradation, indicating its sustainability in future environmental purification prospects.g-C_3N_4-based composite photocatalysts have been widely used in the photocatalytic degradation of various dyes in water. These composites adsorb dyes onto their surfaces and then degrade them under visible light excitation. Combining g-C_3N_4 with other materials to form different types of heterojunction structures can effectively increase the specific surface area, provide more reduction reaction sites, and improve the light response range and charge separation.

3.2 Degradation of antibiotics

Antibiotics are crucial for the treatment of infectious diseases worldwide. However, a large number of antibiotics

Table 3 Information on the degradation of antibiotics by g-C_3N_4-based photocatalyst[a]

Catalyst	Process conditions	Light source	Catalyst dosage	Performance	Active species	Ref
C-doped g-C_3N_4/WO_3	TC: 10 mg/L, 100 mL	500 W Xe lamp (λ > 420 nm)	100 mg	60 min, 75%	$\cdot O_2^-$, **h^+**, ·OH	(Zhao et al. 2021a)
$Bi_2O_2CO_3$/S-doped g-C_3N_4	TC: 10 mg/L	300 W Xe lamp	30 mg	30 min, 82.6%	**h^+**, $\cdot O_2^-$, ·OH	(Liu et al. 2021b)
CeO_2/N-doped CQDs g-C_3N_4	TC: 20 mg/L, 100 mL	300 W Xe lamp (λ > 420 nm)	100 mg	60 min, 100%	$\cdot O_2^-$, **·OH**, h^+, e^-	(Qi et al. 2020)
PNIPAM-Ag/Ag_3PO_4/g-C_3N_4	TC: 20 mg/L, 100 mL	250 W Xe lamp	50 mg	120 min, 88.96%	$\cdot O_2^-$, **h^+**, ·OH	(Sun et al. 2020)
Fe-doped g-C_3N_4	TC: 20 mg/L, 60 mL	300 W Xe lamp	30 mg	80 min, 63.7%	$\cdot O_2^-$, **h^+**, ·OH	(Xu et al. 2019)
g-C_3N_4@ZIF-8	TC: 20 mM, 50 mL	300 W Xe lamp (λ ≥ 430 nm)	10 mg	60 min, 87.6%	$\cdot O_2^-$, **$^1O_2$**, h^+, e^-, ·OH	(Yuan et al. 2021a)
Mo_2C/g-C_3N_4	TC: 20 mg/L, 30 mL	300 W Xe lamp (λ > 420 nm)	30 mg	60 min, 91.6%	$\cdot O_2^-$, **h^+**, ·OH	(Zhang et al. 2020a)
Co_3O_4/g-C_3N_4	TC: 15 mg/L, 100 mL	500 W Xe lamp (λ > 420 nm)	40 mg	150 min, 92.6%	$\cdot O_2^-$, h^+, ·OH	(Zhao et al. 2021c)
g-C_3N_4/Ag/BNQDs	TC: 100 mL	300 W Xe lamp (λ > 420 nm)	50 mg	80.54%, 60 min,	$\cdot O_2^-$, h^+, ·OH	(Ren et al. 2022)
g-C_3N_4/g-C_3N_{4-x}	TC: 20 mg/L, 100 mL	300 W Xe lamp (λ > 420 nm)	50 mg	92.7%, 60 min	$\cdot O_2^-$, h^+, ·OH	(Feng et al. 2023)
Ag/g-C_3N_4	TC: 20 mg/L, 200 mL	300 W Xe lamp(λ ≥ 420 nm)	50 mg	100%, 75 min	$\cdot O_2^-$, **h^+**, ·OH, H_2O_2	(Sun et al. 2022)
AgI/(Na,F) doped g-C_3N_4	TC: 35 mg/L, 100 mL	300 W Xe lamp (λ > 400 nm)	50 mg	21 min	$\cdot O_2^-$, **·OH**, h^+	(Zhou et al. 2021)
g-C_3N_4/CQDs/carbon cloth	CPX: 5 mg/L			60 min, 98%	$\cdot O_2^-$, h^+, ·OH	(Wang et al. 2021e)
Ag_3PO_4/g-C_3N_4	SMX: 1 mg/L, 100 mL	300 W Xe lamp (λ > 400 nm)	5 mg	60 min, 100%	**h^+**, $\cdot O_2^-$, ·OH, $^1O_2$	(Zhou et al. 2017)
g-C_3N_4/Bi_4NbO_8Cl	OTC: 20 mg/L, 10 mL	18 W LED light	10 mg	60 min, 87%	$\cdot O_2^-$, **h^+**, ·OH	(Majumdar et al. 2021)
Co/g-C_3N_4	NOR: 6 mg/L, 30 mL	500 W Xe lamp (λ > 420 nm)	40 mg	10 min, 96.4%	**·OH, $SO_4^{\cdot -}$**	(Zhang et al. 2021d)
CuO-ZnO/g-C_3N_4	amoxicillin: 60 mg/L, 250 mL, pH = 7	300 W Xe lamp	225 mg	120 min, 100%	**·OH**, $\cdot O_2^-$, h^+, e^-	(Moradi et al. 2021)
UiO-66/NH_2-MIL-125/g-C_3N_4	OFX: 20 mg/L	300 W Xe lamp (λ > 420 nm)	0.1 g/L	99.1%, 50 min	$\cdot O_2^-$, **·OH**, h^+, e^-	(Sepehrmansourie et al. 2023)
$BiVO_4$/g-C_3N_4/$NiFe_2O_4$	OFX: 10 mg/L, 100 mL, pH = 9	300 W Xe lamp (λ > 420 nm)	100 mg	20 min, 93.8%	**h^+**, $\cdot O_2^-$, ·OH, e^-, $^1O_2$	(Zhao et al. 2021b)
$LaFeO_3$/g-C_3N_4/$BiFeO_3$	CIP: 10 mg/L, 50 mL, pH = 6.3	300 W Xe lamp	20 mg	60 min, 98.6%	$\cdot O_2^-$, h^+, ·OH	(Saravanakumar and Park 2021)

[a] The main active species in each reference are shown boldly in the table

are discharged into aquatic and terrestrial ecosystems, which has become a serious problem. Table 3 lists the recent articles on g-C_3N_4-based materials in antibiotic degradation. As an economic and effective method to deal with antibiotic pollution, photocatalysis technology has attracted extensive attention.

The photocatalytic degradation efficiency of a single photocatalyst can be improved by changing the crystallinity, lattice vacancy, and other methods. For example, three g-C_3N_4 with different crystallinity were prepared by thermal polymerization using urea, thiourea, and melamine as precursors (Phoon et al. 2022). The g-C_3N_4 prepared from melamine, thiourea, and urea precursor were labeled MGCN, TGCN, and UGCN, respectively. According to the XRD analysis, the photocatalysts prepared with three precursors were successfully prepared. Compared with the other two materials, MGCN had higher crystallinity than the other two materials, because melamine formed an ordered melem intermediate, which was conducive to charge carrier migration. All of them were mesoporous materials with paralleled plate narrow pore structures. Due to abundant ammonia released by urea during thermal polymerization, UGCN had a larger surface area and a larger pore size than the other two samples. It can be seen from XPS that the C-S-C peak appeared in the C 1 s of the TGCN sample due to the presence of S in thiourea, suggesting that S was combined with the GCN structure. The authors also pointed out that the carbon/nitrogen ratio of MGCN was 0.697, while that of TGCN and UGCN were 0.650 and 0.668, respectively, which confirms the existence of N defects in MGCN. TGCN exhibited the strongest optical absorption capacity in the UV range, and MGCN showed better optical absorption than UGCN in 400–600 nm. The smallest band gap of TGCN was 2.61 eV, the MGCN was 2.63 eV, and the UGCN was 2.91 eV, indicating that the introduction of S atoms enhanced its light absorption ability. The CB of MGCN, TGCN, and UGCN was − 0.33, − 0.91, and − 0.66 V (vs. NHE), the CB potential of MGCN was more negative than (O_2/•O_2^-), and the VB potential of MGCN was more positive than (H_2O/•OH), indicating that during the photodegradation for MGCN, O_2 reduction and water oxidation can occur at the same time. However, the VB of TGCN and UGCN was more negative than the water oxidation potential, which meant that water oxidation would not happen. MGCN showed the highest photoactivity in the photocatalytic degradation of TC, because the dense structure promoted charge transfer and reduced the band gap. In addition, the presence of nitrogen vacancies prevented rapid charge recombination and promoted more charge migration on the surface of the MGCN. Therefore, it removed 99.5% of TC in 240 min, while the TC removal rates of TGCN and UGCN were only 85.1% and 94.3%. The photodegradation mechanism for MGCN was explored. In the presence of benzoquinone (BQ), ethylenediaminetetraacetic acid disodium (EDTA), and isopropyl alcohol (Jaleh et al. 2021), talhe degradation inhibition rates of TC were 84.8%, 74.8%, and 60.5%, respectively. Hence, the superoxide group was the most effective species to degrade TC. The degradation process was:

$$
\begin{aligned}
GCN \xrightarrow{h\upsilon} GCN(e^- + h^+)\\
e^- + O_2 \rightarrow \cdot O_2^-\\
2H^+ + \cdot O_2^- \rightarrow 2 \cdot OH\\
H_2O + h^+ \rightarrow \cdot OH + H^+\\
TC + \cdot O_2^- \rightarrow Photodegraded\ products\\
TC + \cdot OH \rightarrow Photodegraded\ products\\
TC + h^+ \rightarrow Photodegraded\ products
\end{aligned}
$$

MGCN exhibited the strongest photocatalytic activity. This is because of its relatively small band gap and high crystallinity promoted visible light absorption and rapid migration of carriers. At the same time, the defects generated by nitrogen vacancies can effectively slow down charge recombination.

The built-in electric field generated by the formation of Z-type heterojunctionin in composite materials accelerates charge separation and improves the photocatalytic performance of photocatalysts. For example, nano flowers like $NaBiO_3$ (NBO) supported by 2D g-C_3N_4 with Z-type heterojunction were prepared through a simple hydrothermal method (Wu et al. 2021). $NaBiO_3{\cdot}2H_2O$ and a certain amount of CN were added into the NaOH solution, and hydrothermally treated at 120 °C for 12 h. XRD results showed that the peak of NBO retained in the g-C_3N_4/$NaBiO_3$ (CN/NBO) photocatalyst, which indicated that g-C_3N_4 did not affect the crystal structure of NBO. The morphology of composites studied by SEM showed that g-C_3N_4 was a 2D nanosheet, while NBO was a 3D nanoflower. The smaller NBO was tightly combined on the surface of g-C_3N_4 in the composite, which further confirmed the successful construction of CN/NBO heterostructure. Photocatalytic experiments were carried out on the prepared materials with tetracycline as the target pollutant. With the addition of the percentage of g-C_3N_4 in the composite, the degradation efficiency of the composite first increased and then decreased. The degradation efficiency of the composite with 5% of CN was the highest. In addition, the photocatalyst still degraded 80% of TC in the eighth degradation. The photocatalyst used for 8 times was tested by XRD. The obvious characteristic peaks of CN and NBO could still be found in the sample after eight runs, which proved

the stability of the composite material. To clarify the mechanism of photocatalytic degradation, IPA, p-benzoquinone (PBQ), and ethylenediaminetetraacetic acid disodium (EDTA-2Na) were used to test the active species in the reaction process. The degree of inhibition on tetracycline degradation was IPA > PBQ > EDTA-2Na, which showed that •OH played a key role in the degradation process, followed by $\bullet O_2^-$ and h^+. The corresponding reactions were as follows:

$$CN/NBO + h\upsilon \rightarrow CN/NBO(e^- + h^+)$$
$$e^- + O_2 \rightarrow \cdot O_2^-$$
$$\cdot O_2^- + 2H^+ + e^- \rightarrow H_2O_2$$
$$h^+ + OH^- \rightarrow \cdot OH$$
$$H_2O_2 + e^- \rightarrow \cdot OH + OH^-$$
$$TC + \cdot OH + \cdot O_2^- + h^+ \rightarrow CO_2 + H_2O + degradation\ products$$

The built-in electric field of the Z-type heterojunction photocatalyst prepared by the hydrothermal method was conducive to accelerating charge separation and providing a higher redox potential for the carrier to form free radicals. Therefore, more active groups were formed on CN/NBO to degrade tetracycline, which provided an effective method for antibiotic degradation.

A similar method can also be used to prepare a ternary photocatalyst. For example, An indirect Z-type nitrogen-doped carbon dots (NCD) modified Bi_2MoO_6/g-C_3N_4 ternary photocatalyst (NCD@BMCN) was prepared by hydrothermal method (Dang et al. 2021). NCD was obtained by hydrothermal treatment of the mixture of citric acid and Ethylenediamine solution at 160 °C for 4 h. Then, g-C_3N_4 nanosheets (CN) were obtained by calcining urea at 500 °C for 2 h. Bi_2MoO_6/g-C_3N_4 (BMCN) was synthesized by hydrothermal method. $Bi(NO_3)_3{\cdot}5H_2O$ and $Na_2MoO_4{\cdot}2H_2O$ were dissolved in diethylene glycol solution, then CN dispersed in ethanol was added. The mixture was hydrothermally reacted at 160 °C for 4 h to obtain a yellow BMCN precipitate. Finally, the prepared NCD solution was added to the BMCN suspension and stirred for 24 h. The prepared product was washed and vacuum dried to obtain NCD@BMCN. The 10–20 nm NCDs were uniformly deposited on the surface of BMCN in NCD@BMCN, which increased specific surface area, photocurrent density, and charge transfer efficiency. The existence of NCD on the hexagonal diffraction plane of the internal region of sp^2 graphite carbon was confirmed from its fast Fourier transform (FFT) image, indicating that NCD particles, Bi_2MoO_6 rods, and CN nanosheets were well combined to form heterostructures. The UV–Vis spectra showed that the absorption edge of BMCN had a red shift relative to pure g-C_3N_4 due to the narrower band gap of Bi_2MoO_6 compared with that of g-C_3N_4. The addition of NCD further expanded its visible light absorption range and significantly improved the light absorption capacity. NCD@BMCN removed 99% of CIP under visible light in 30 min compared with BMCN (65%) and g-C_3N_4 (20%). The photodegradation efficiency of CIP by different photocatalysts was simulated by pseudo-first-order equation. The pseudo-first-order rate constant of NCD@BMCN was 3.4 times and 15 times higher than that of BMCN and CN, respectively, which proved that NCD played a key role in improving photocatalytic efficiency. To reveal its photocatalytic degradation mechanism, tert-butanol (t-BuOH) and 1,4 benzoquinone (1,4-BQ) were added to the solution. The removal efficiency of CPX was significantly reduced, indicating that •OH and $\bullet O_2^-$ were the main active species. In addition, after the addition of ammonium oxalate monohydrate (AO), the photocatalytic efficiency did not decrease significantly, indicating that the h^+ contributed little to the photocatalytic degradation. The degradation mechanism was as follows:

$$NCD@BMCN + h\upsilon \rightarrow e^- + h^+$$
$$OH^- + h^+ \rightarrow \cdot OH$$
$$O_2 + e^- \rightarrow \cdot O_2^-$$
$$\cdot O_2^- + H_2O \rightarrow \cdot OOH + OH$$
$$\cdot OOH + H^+ + e^- \rightarrow 2 \cdot OH$$

Under the visible light irradiation condition, the ternary photocatalyst showed good degradation ability for CPX, owing to the uniform distribution of BMO nanorods on the CN nanosheets and the increased specific surface area of the composite material. The NCD@BMCN showed a Z-scheme mechanism with photoinduced e^- moving from the CB of Bi_2MoO_6 to the VB of CN, thereby generating more photogenerated carriers and enhancing the photocatalytic performance of CIP degradation.

Generally, g-C_3N_4-based photocatalysts have been widely used in antibiotic degradation. However, the degradation effect of a single g-C_3N_4 photocatalyst on antibiotics is limited. By changing the crystallinity and introducing lattice vacancies of g-C_3N_4, its photocatalytic ability to degrade antibiotics can be improved by increasing carriers' mobility and slowing charges' recombination. Moreover, the internal electric field in g-C_3N_4 heterostructure photocatalysts accelerates charge separation, thereby promoting antibiotic degradation. These methods effectively enhance the photocatalytic degradation abilities of g-C_3N_4 for antibiotics and provide ideas for controlling antibiotic pollution.

3.3 Degradation of phenols

The applications of g-C_3N_4-based photocatalysts have also been proposed for phenolic degradation. Table 4 lists the recent applications of g-C_3N_4-based photocatalysts

Table 4 Information on the degradation of phenols by g-C_3N_4-based photocatalyst[a]

Catalyst	Process conditions	Light source	Catalyst dosage	Performance	Active species	Ref
Fe_2O_3/g-C_3N_4@N-TiO_2	BPA: 4.5 mg/L, 200 mL pH = 3	249 W Xe lamp	40 mm × 25 mm	40 min, 100%	**•OH**, $\cdot O_2^-$	(Kong et al. 2020)
g-C_3N_4-ThA_x	BPA: 10 mg/L	300 W Xe lamp ($\lambda \geq 420$ nm)		100 min, 98.8%	$\cdot O_2^-$, **h^+**, •OH	(Ge et al. 2021)
In_2O_3/O doped g-C_3N_4	BPA: 50 mg/L, 50 mL pH = 5	Xe lamp ($\lambda > 420$ nm)	50 mg	180 min, 91%	$\cdot O_2^-$, h^+, •OH	(Uddin et al. 2021)
CeO_2/g-C_3N_4	BPA:10 mg/L, 100 mL	500 W xenon lamp	100 mg	150 min, 94.1%	**•OH**, $\cdot O_2^-$, h^+	(Zhao et al. 2021d)
S, K-doped g-C_3N_4	BPA: 10 mg/L, 50 mL	300 W lamp ($\lambda > 420$ nm)	15 mg	100 min, 64%	**•OH, h^+**, $\cdot O_2^-$, $^1O_2$, e^-	(Xu et al. 2022)
CdSe-quantum dots coupled P doped-g-C_3N_4	2,4-DCP: 10 mg/L, 80 mL	300 W Xe lamp ($\lambda > 420$ nm)	50 mg	60 min, 78%	$\cdot O_2^-$, h^+, •OH	(Raziq et al. 2020)
$BiFeO_3$-g-C_3N_4-WO_3	2,4-DCP: 20 mg/L, 40 mL	300 W Xe lamp	100 mg	60 min, 63%	**•OH,** h^+, e^-	(Ali et al. 2020)
g-C_3N_4/8-quinolinolato iron(III) (Q_3Fe)/H_2O_2	2,4-DCP: 30 mg/L	300 W lamp ($\lambda > 400$ nm)	20 mg	80 min, 90%	**•OH**, $\cdot O_2^-$	(Feng et al. 2017b)
g-C_3N_4/8-quinolinolato iron(III) (Q_3Fe)/H_2O_2	ACE: 3 mg/L, 50 mL	300 W Xe lamp	25 mg	25 min, 80%	$\cdot O_2^-$, $^1O_2$, •OH	(Li et al. 2021a)
CeO_2/I-K doped g-C_3N_4	ACE: 10 mg/L, 20 mL pH = 11	Eight 8 W visible light lamps ($\lambda = 465 \pm 40$ nm)	40 mg	120 min, 98%	$\cdot O_2^-$, h^+, •OH	(Paragas et al. 2021)
g-C_3N_4/WO_3	PNP: 10 mg/L, 50 mL	300 W Xe lamp	50 mg	90 min, 100%	$\cdot O_2^-$, h^+, •OH	(Zhang et al. 2021e)
α-Fe_2O_3/g-C_3N_4	PNP: 389.5 mg/L, 100 mL pH = 3 H_2O_2	160 W incandescent lamp ($400 < \lambda < 780$ nm)	200 mg	120 min	**•OH**, $\cdot O_2^-$, h^+	(Sun et al. 2021a, b)
$Zn_{1-1.5x}Fe_xS$/g-C_3N_4	PNP: 10 mg/L, 250 mL	500 W lamp	200 mg	120 min, 96%	**•OH**, $\cdot O_2^-$, h^+, e^-	(Wang et al. 2020)
g-C_3N_4/ZnO	4-CP: 9.4 mg/L, 100 mL	300 W lamp ($\lambda > 420$ nm)	100 mg	60 min, 95%	**•OH,** $\cdot O_2^-$, h^+	(Wang et al. 2017)
g-C_3N_4/perylene tetracarboxylic diimide -Br	4-CP: 5 mg/L	$\lambda > 254$ nm	50 mg	60 min, 100%	**•OH**, **$\cdot O_2^-$,** h^+	(Liu et al. 2021a)
$[Mo_7O_{24}]^{6-}$/g-C_3N_4	4-CP; BPA	Xe lamp ($\lambda > 420$ nm)		80 min, 100%; 30 min, 100%	$\cdot O_2^-$, h^+**,** •OH	(Zhang et al. 2022a)
g-C_3N_4-OH/Ov-TiO_2	Phenol: 20 mg/L, 50 mL	300 W Xe lamp ($\lambda \geq 420$ nm)	50 mg	220 min, 100%	**•OH,** $\cdot O_2^-$, h^+	(Ma et al. 2021a)
TiO_2/B-doped g-C_3N_4	Phenol: 20 mg/L, 20 mL	250 W visible light	20 mg	120 min, 87%	**h^+**, **•OH**, $\cdot O_2^-$, e^-	(Behera et al. 2021)
N doped g-C_3N_4	Phenol: 10 mg/L	300 W lamp ($\lambda > 420$ nm)	1 g/L	180 min, 70.1%	$\cdot O_2^-$, h^+, •OH	(Zhu and Zhou 2021)
Bi_2Se_3/g-C_3N_4	Phenol: 100 mg/L, 15 mL	60 W LED lamp ($\lambda > 400$ nm)	50 mg	180 min	$\cdot O_2^-$, •OH, h^+	(He et al. 2022a)

[a] The main active species in each reference are shown boldly in the table

for phenolic removal. Modification of g-C_3N_4 by doping and introducing defects are effective ways to improve the photocatalytic effect of g-C_3N_4. Modified g-C_3N_4 was synthesized by thermal polymerization using urea as raw material and EDTA-2Na as a modifier to degrade BPA (He et al. 2022b). In XRD patterns, the (002) peaks of g-C_3N_4 were shifted to lower angles and widened with the increasing of EDTA-2Na addition, suggesting that the presence of EDTA-2Na slightly disturbed the in-plane structural packing of g-C_3N_4. Through FTIR spectra results, when the amount of EDTA-2Na reached a certain value, the signals of tri-s-triazine units and aromatic C-N heterocycles became small, confirming that the in-plane structure accumulation was disordered by EDTA-2Na.

The morphology of the materials was studied by SEM. The original g-C_3N_4 showed a bulk and agglomerated structure, while modified g-C_3N_4 showed a loose wrinkled structure, which might be due to the fact that the introduction of EDTA-2Na led to uneven distribution of electron density. In addition, the modified g-C_3N_4 had a larger specific surface area, suggesting that it had more photocatalytic activity sites. On the other hand, XPS results showed that the presence of EDTA-2Na increased carbon content and might cause defects, suggesting that the presence of EDTA-2Na disturbed the planar structure of g-C_3N_4. Compared with g-C_3N_4, the edge of the absorption band of the modified g-C_3N_4 sample showed an obvious red shift. In addition, with the increase of EDTA-2Na content, the doping of carbon in the g-C_3N_4 framework led to the broadening of the absorption band, indicating that the absorption range of light expanded. At the same time, the band gap energy of g-C_3N_4 was also reduced. In addition, modified g-C_3N_4 impressively achieved 98.6% BPA photodegradation after 150 min when the original g-C_3N_4 degraded only 39.6%. To clarify the strong photocatalytic ability of modified g-C_3N_4 composites, the mechanism of charge transfer was presented. According to the characterization results, the combination of C doping and defects on g-C_3N_4 can broaden the optical adsorption scope, improve the transfer of carriers, and reduce the recombination of e^- and h^+. Under optical irradiation, abundant photoinduced e^- and h^+ were produced. The e^- also moved to the surface and reacted with oxygen to form $\bullet O_2^-$. In addition, $\bullet O_2^-$ and h^+ produced by modified g-C_3N_4 played an important role in the photocatalytic degradation of BPA. C doping and defects reduced the band gap of g-C_3N_4 and accelerated the migration of photogenerated carriers, which made the modified g-C_3N_4 produce more excited electrons under visible light excitation and enhanced the separation ability of photogenerated electron holes, resulting in a significant enhancement of photocatalytic effect.

Combining g-C_3N_4 with other materials is another effective method to improve the photocatalytic activity of g-C_3N_4 in the degradation of phenols. For example, CeO_2/g-C_3N_4 composites were prepared using a wet chemical solution method (Humayun et al. 2019). g-C_3N_4 was obtained by calcining dicyandiamide at 550 °C in the air for 2 h. The solution of cerium nitrate and ammonia was hydrothermally reacted at 160 °C for 12 h and further calcined at 500 °C for 2 h to obtain CeO_2. Then, g-C_3N_4 and a certain amount of CeO_2 were dispersed in a mixed solvent of ethanol and water, stirred and dried to remove the solvent. Finally, the dried product was annealed in air at 500 °C for 2 h to obtain CeO_2/g-C_3N_4 with different amounts of CeO_2. XRD results showed that the diffraction peaks of CeO_2 appeared in the composites. With the increase of CeO_2 content in composites, the peak intensity gradually increased and shifted to a larger direction of 2θ, indicating that g-C_3N_4 and CeO_2 were successfully coupled. The SEM images showed that the small size CeO_2 nanoparticles were wrapped by layered g-C_3N_4 irregular particles, and the particles became clearer as the amount of CeO_2 increased. The TEM results showed that CeO_2 particles were well dispersed on the surface of g-C_3N_4. In addition, the selective area electron diffraction images confirmed that CeO_2 existed in the form of nanocrystals. Therefore, a heterojunction was formed between CeO_2 and g-C_3N_4, which facilitated the migration of electrons between the two particles. The photocatalytic test of the composite material showed that g-C_3N_4 degraded 29% and CeO_2 degraded 34% of 2,4-DCP after irradiation for 2 h, which was attributed to the small particle size with more active sites and higher specific surface area. After the coupling of the two, the photocatalytic effect was significantly improved. The composite material with 15% CeO_2 content had the best activity, which degraded 57% of 2,4-DCP in 2 h, while the photocatalytic efficiency of composite material with 20% CeO_2 content was slightly reduced. This is because the excessive CeO_2 acted as the recombination center of the charge carrier, resulting in a decrease in the photocatalytic effect. In addition, the cycle test showed that the photocatalytic activity of the composite did not change after 4 cycles, indicating that the photocatalyst had good stability. The CeO_2/g-C_3N_4 scavenger trapping test found that •OH was the main active material and the effects of $\bullet O_2^-$ and h^+ were relatively small, and the degradation steps were as follows:

$$CeO_2/CN + h\upsilon \rightarrow CeO_2(e^- + h^+)/CN(e^- + h^+)$$
$$CeO_2(e^- + h^+)/CN(e^- + h^+) \rightarrow CeO_2(e^- + e^-)/CN(h^+ + h^+)$$
$$e^- + O_2 \rightarrow \cdot O_2^-$$
$$2e^- + 2H^+ + \cdot O_2^- \rightarrow \cdot OH + OH^-$$
$$\cdot O_2^- + 2{,}4 - DCP \rightarrow intermediates \rightarrow degradation\ products$$
$$\cdot OH + 2{,}4 - DCP \rightarrow intermediates \rightarrow degradation\ products$$
$$h^+ + 2{,}4 - DCP \rightarrow intermediates \rightarrow degradation\ products$$

Compared with bare g-C_3N_4, the photocatalytic activity of the composite was significantly enhanced because the two components had a suitable energy platform that promoted the separation and migration of charge carriers.

The formation of double Z-type heterojunctions by preparing ternary compounds to promote the photocatalytic activity of photocatalysts has also attracted wide attention. A novel ternary g-C_3N_4/Bi_2MoO_6/CeO_2 (CBC) nanocomposite was prepared by solid-phase pyrolysis-assisted ultrasonic dispersion method for the degradation of 4-CP (Gao et al. 2022). The microstructure of the synthesized samples was observed by SEM and TEM. The original CeO_2 was spherical, and

Bi_2MoO_6 nanosheets were homogeneously wrapped on the surface of CeO_2 microspheres. The g-C_3N_4 had an ultra-thin layered structure after the two-step polymerization of melamine. Atomic force microscopy (AFM) analysis showed that the average thickness of the g-C_3N_4 nanosheets was less than 5 nm. This structure can not only increase the surface active sites, but also expand the light response range and facilitate the transport of photogenerated carriers. The TEM images of CBC composites showed that the Bi_2MoO_6/CeO_2 was successfully anchored on the g-C_3N_4 and formed a close interfacial contact, which facilitated the effective transfer of photogenerated charge between different nanostructures. In addition, CBC exhibited a larger light response range. The CBC showed the highest degradation efficiency of 99.1% for 4-CP. A reaction mechanism was proposed for the enhanced photocatalytic performance. The e^- and h^+ of g-C_3N_4, Bi_2MoO_6, and CeO_2 were generated on CB and VB, respectively. Combined with XPS analysis, the photoexcited e^- in the CB of Bi_2MoO_6 can be transferred to the VB of g-C_3N_4 and CeO_2, respectively, consuming the above h^+ to achieve photogenerated carrier separation. The h^+ on Bi_2MoO_6 VB can directly degrade 4-CP, while the e^- left in CB of g-C_3N_4 and CeO_2 can quickly react with O_2 to form $\bullet O_2^-$. In addition, some $\bullet O_2^-$ was converted to •OH. Finally, 4-CP was synergistically degraded by reactive radicals such as $\bullet O_2^-$, h^+, and •OH. Therefore, the ternary heterojunction and double Z-type charge transport mechanism were formed in the CBC nanocomposites. Through simple solid-state thermal decomposition assisted ultrasonic dispersion, the spherical Bi_2MoO_6/CeO_2 was uniformly dispersed on the g-C_3N_4 nanosheets, and a double Z-type heterojunction was formed by close interface contact, which realized the effective separation of electron–hole pairs and promoted the activity of the photocatalyst.

Thus, g-C_3N_4-based photocatalyst has been widely used in the degradation of phenolic pollutants. Under the light irradiation, the electrons on the VB migrate to the CB, and photogenerated electrons and holes will further react to generate active free radicals for phenolic pollutants degradation. In conclusion, introducing defects and preparation of Z-type heterojunction material are effectively strategies for improving the photodegradation ability of g-C_3N_4 for phenolic pollutants.

4 Conclusions and perspectives

In the present review, we highlight the applications of g-C_3N_4 and its derivatives in the photodegradation of organic pollutants in water. The g-C_3N_4-based photocatalysts have the advantages of high efficiency, saving energy, and reusability, making them promising photocatalysts for environmental applications, especially with respect to organic pollutant photodegradation. Further investigations thus should be conducted to promote research in this field and fill following important knowledge gaps. 1) Previous studies have mainly concentrated on improving the photodegradation activity of g-C_3N_4-based materials under laboratory experimental conditions. The degradation activity and mechanism for organic pollutants in the actual industrial wastewater are still unclear. 2) The applicability of g-C_3N_4 photodegradation technique under natural conditions needs to be further evaluated. 3) Obstacles have yet to be addressed for the upscale from laboratory to commercially available photocatalytic wastewater treatment technology. 4) Most of the relevant laboratory studies have only focused on the removal of one pollutant at a time. However, it rarely happens in real wastewater, which usually contains various pollutants including both easily degradable and recalcitrant ones.

Abbreviations

4-CP	4-Chlorophenol
4-NP	4-Nitrophenol
2,4-DCP	2,4-Dichlorophenol
ACE	Acetaminophen
AO7	Acid Orange 7
BPA	Bisphenol A
CPX	Ciprofloxacin
CQDs	Carbon quantum dots
CR	Congo red
MB	Methylene blue
MG	Malachite green
MO	Methyl orange
NOR	Norfloxacin
OFX	Ofloxacin
OTC	Oxytetracycline
PNP	P-nitrophenol
RhB	Rhodamine B
SMX	Sulfamethoxazole
TC	Tetracycline
ThA	3-Thiophenemalonic acid

Acknowledgements

This work was funded by the National Natural Science Foundation of China (12264030), the Key Project of Key Research and Development Program of Jiangxi Province (20212BBE51021), Natural Science Foundation of Jiangxi Province (20224BAB204023).

Authors' contributions

Yidan Luo: Writing-Review and Editing, Visualization, Project administration, Funding acquisition. Yaowei Zhu, Yu Han, Huiyin Ye, Ruochen Liu, Yuanwang Lan, Shuohan Yu, Longshuai Zhang, Zuozhu Yin & Xianchuan Xie: Writing-Review and Editing. Mingshan Xue & Bin Gao: Creating the idea, Writing-Review and Editing, Supervision, Project administration. The authors read and approved the final manuscript.

Funding

Not applicable.

Availability of data and materials

The data are available from the corresponding author on reasonable request.

Declarations

Competing interests
The authors declare no competing interests.

Author details
[1]Key Laboratory for Microstructural Control of Metallic Materials of Jiangxi Province, School of Materials Science and Engineering, Nanchang Hangkong University, Nanchang 330063, China. [2]Key Laboratory of Poyang Lake Environment and Resource Utilization, Ministry of Education, School of Resource and Environment, Nanchang University, Nanchang 330031, P. R. China. [3]School of Environmental and Chemical Engineering, Nanchang Hangkong University, Nanchang 330063, China. [4]Key Laboratory of Jiangxi Province for Persistent Pollutants Control and Resources Recycle, Nanchang Hangkong University Nanchang, Jiangxi 330063, P. R. China. [5]Department of Agricultural and Biological Engineering, University of Florida, Gainesville, FL 32611, USA.

Received: 7 October 2022 Revised: 24 February 2023 Accepted: 3 March 2023
Published online: 06 April 2023

References
Abu-Sari SM, Daud W, Patah MFA, Ang BC (2022) A review on synthesis, modification method, and challenges of light-driven H_2 evolution using g-C_3N_4-based photocatalyst. Adv Colloid Interface Sci 307:102722

Aghdam SM, Haghighi M, Allahyari S, Yosefi L (2017) Precipitation dispersion of various ratios of BiOI/BiOCl nanocomposite over g-C_3N_4 for promoted visible light nanophotocatalyst used in removal of acid orange 7 from water. J Photochem Photobiol A Chem 338:201–212

Ali S, Humayun M, Pi W, Yuan Y, Wang M, Khan A, Yue P, Shu L, Zheng Z, Fu Q, Luo W (2020) Fabrication of $BiFeO_3$-g-C_3N_4-WO_3 Z-scheme heterojunction as highly efficient visible-light photocatalyst for water reduction and 2,4-dichlorophenol degradation: Insight mechanism. J Hazard Mater 397:122708

Amanulla B, Sannasi S, Abubakker AKM, Ramaraj SK (2018) A magnetically recoverable bimetallic Au-FeNPs decorated on g-C_3N_4 for efficient photocatalytic degradation of organic contaminants. J Mol Liq 249:754–763

Bai X, Yan S, Wang J, Wang L, Jiang W, Wu S, Sun C, Zhu Y (2014) A simple and efficient strategy for the synthesis of a chemically tailored g-C_3N_4 material. J Mater Chem A 2:17521–17529

Behera A, Babu P, Parida K (2021) Growth of macroporous TiO_2 on B-doped g-C_3N_4 nanosheets: a Z-scheme photocatalyst for H_2O_2 production and phenol oxidation under visible light. Inorg Chem Front 8:1489–1499

Benisti I, Shaik F, Xing Z, Ben-refael A, Amirav L, Paz Y (2021) The effect of Pt cocatalyst on the performance and transient IR spectrum of photocatalytic g-C_3N_4 nanospheres. Appl Surf Sci 542:148432

Biswal BK, Balasubramanian R (2022) Adsorptive removal of sulfonamides, tetracyclines and quinolones from wastewater and water using carbon-based materials: recent developments and future directions. J Clean Prod 349:131421

Chandra S, Jagdale P, Medha I, Tiwari AK, Bartoli M, Nino A et al (2021) Biochar-supported TiO_2-based nanocomposites for the photocatalytic degradation of sulfamethoxazole in water-a review. Toxics 9:313

Chu Y-C, Lin T-J, Lin Y-R, Chiu W-L, Nguyen B-S, Hu C (2020) Influence of P, S, O-Doping on g-C_3N_4 for hydrogel formation and photocatalysis: an experimental and theoretical study. Carbon 169:338–348

Cui J, Qi D, Wang X (2018) Research on the techniques of ultrasound-assisted liquid-phase peeling, thermal oxidation peeling and acid-base chemical peeling for ultra-thin graphite carbon nitride nanosheets. Ultrason Sonochem 48:181–187

Dang VD, Adorna J, Annadurai T, Bui TAN, Tran HL, Lin L-Y, Doong R-A (2021) Indirect Z-scheme nitrogen-doped carbon dot decorated Bi_2MoO_6/g-C_3N_4 photocatalyst for enhanced visible-light-driven degradation of ciprofloxacin. Chem Eng J 422:130103

Danish M, Muneer M (2021) Excellent visible-light-driven Ni-ZnS/g-C_3N_4 photocatalyst for enhanced pollutants degradation performance: Insight into the photocatalytic mechanism and adsorption isotherm. Appl Surf Sci 563:150262

Darie M, Seftel EM, Mertens M, Ciocarlan RG, Cool P, Carja G (2019) Harvesting solar light on a tandem of Pt or Pt-Ag nanoparticles on layered double hydroxides photocatalysts for p-nitrophenol degradation in water. Appl Clay Sci 182:105250

Dong F, Zhao Z, Xiong T, Ni Z, Zhang W, Sun Y, Ho WK (2013) In situ construction of g-C_3N_4/g-C_3N_4 metal-free heterojunction for enhanced visible-light photocatalysis. ACS Appl Mater Inter 5:11392–11401

Ehsan MF, Shafiq M, Hamid S, Shafiee A, Usman M, Khan I, Ashiq MN, Arfan M (2020) Reactive oxygen species: New insights into photocatalytic pollutant degradation over g-C_3N_4/ZnSe nanocomposite. Appl Surf Sci 532:147418

Fauzi AA, Jalil AA, Hassan NS, Aziz FFA, Azami MS, Hussain I, Saravanan R, Vo DN (2022) A critical review on relationship of CeO_2-based photocatalyst towards mechanistic degradation of organic pollutant. Chemosphere 286:131651

Feng D, Cheng Y, He J, Zheng L, Shao D, Wang W, Wang W, Lu F, Dong H, Liu H, Zheng R, Liu H (2017a) Enhanced photocatalytic activities of g-C_3N_4 with large specific surface area via a facile one-step synthesis process. Carbon 125:454–463

Feng W, Zhang L, Fang J, Lu S, Wu S, Chen Y, Fang Z (2017b) Improved photodegradation efficiency of 2,4-DCP through a combined Q_3Fe(III))-decorated porous g-C_3N_4/H_2O_2 system. Water Air Soil Poll 228:1–11

Feng G, Mingyang L, Hongji R, Xiliu H, Keke S, Weilong S, Changyu L (2019) Facile bottom-up preparation of Cl-doped porous g-C_3N_4 nanosheets for enhanced photocatalytic degradation of tetracycline under visible light. Sep Purif Technol 228:115770

Feng C, Ouyang X, Deng Y, Wang J, Tang L (2023) A novel g-C_3N_4/g-C_3N_{4-x} homojunction with efficient interfacial charge transfer for photocatalytic degradation of atrazine and tetracycline. J Hazard Mater 441:129845

Fujishima A, Honda K (1972) Electrochemical photolysis of water at a semiconductor electrode. Nature 238:37–38

Gao S, Wang X, Song C, Zhou S, Yang F, Kong Y (2021) Engineering carbon-defects on ultrathin g-C_3N_4 allows one-pot output and dramatically boosts photoredox catalytic activity. Appl Catal B-Environ 295:120272

Gao Q, Wang Z, Li J, Liu B, Liu C (2022) Facile synthesis of ternary dual Z-scheme g-C_3N_4/Bi_2MoO_6/CeO_2 photocatalyst with enhanced 4-chlorophenol removal: Degradation pathways and mechanism. Environ Pollut 314:120436

Ge L, Han C, Liu J, Li Y (2011) Enhanced visible light photocatalytic activity of novel polymeric g-C_3N_4 loaded with Ag nanoparticles. Appl Catal A Gen 409–410:215–222

Ge F, Huang S, Yan J, Jing L, Chen F, Xie M, Xu Y, Xu H, Li H (2021) Sulfur promoted n-π* electron transitions in thiophene-doped g-C_3N_4 for enhanced photocatalytic activity. Chinese J Catal 42:450–459

Guo X, Duan J, Wang W, Zhang Z (2020) Modified graphitic carbon nitride as the photocatalyst for wastewater treatment under visible light irradiation. Fuel 280:118544

Gupta VK, Suhas, (2009) Application of low-cost adsorbents for dye removal–a review. J Environ Manage 90:2313–2342

He R, Ou S, Liu Y, Liu Y, Xu D (2022a) In situ fabrication of Bi_2Se_3/g-C_3N_4 S-scheme photocatalyst with improved photocatalytic activity. Chinese J Catal 43:370–378

He X, Lei L, Wen J, Zhao Y, Cui L, Wu G (2022b) One-pot synthesis of C-doping and defects co-modified g-C_3N_4 for enhanced visible-light photocatalytic degradation of bisphenol A. J Environ Chem Eng 10:106911

Hou H, Zhang X (2020) Rational design of 1D/2D heterostructured photocatalyst for energy and environmental applications. Chem Eng J 395:125030

Hou J, Jiang T, Wang X, Zhang G, Zou J-J, Cao C (2021) Variable dimensional structure and interface design of g-C_3N_4/BiOI composites with oxygen vacancy for improving visible-light photocatalytic properties. J Clean Prod 287:125072

Hu X, Zheng W, Yong Y, Xu Y, Wang X, Yao X (2020) One-step synthesis of iodine-doped g-C_3N_4 with enhanced photocatalytic nitrogen fixation performance. Appl Surf Sci 510:145413

Huang J, Li D, Li R, Zhang Q, Chen T, Liu H, Liu Y, Lv W, Liu G (2019) An efficient metal-free phosphorus and oxygen co-doped g-C_3N_4 photocatalyst with enhanced visible light photocatalytic activity for the degradation of fluoroquinolone antibiotics. Chem Eng J 374:242–253

Humayun M, Hu Z, Khan A, Cheng W, Yuan Y, Zheng Z, Fu Q, Luo W (2019) Highly efficient degradation of 2,4-dichlorophenol over CeO_2/g-C_3N_4 composites under visible-light irradiation: Detailed reaction pathway and mechanism. J Hazard Mater 364:635–644

Jaleh B, Nasrollahzadeh M, Mohazzab BF, Eslamipanah M, Sajjadi M, Ghafuri H (2021) State-of-the-art technology: recent investigations on laser-mediated synthesis of nanocomposites for environmental remediation. Ceram Int 47:10389–10425

Jiang J, Mu Z, Zhao P, Wang H, Lin Y (2020) Photogenerated charge behavior of BiOI/g-C_3N_4 photocatalyst in photoreduction of Cr (VI): a novel understanding for high-performance. Mater Chem Phys 252:123194

Kiernan JA (2001) Classification and naming of dyes, stains and fluorochromes. Biotech Histochem 76:261–278

Kong X, Li J, Yang C, Tang Q, Wang D (2020) Fabrication of Fe_2O_3/g-C_3N_4@N-TiO_2 photocatalyst nanotube arrays that promote bisphenol A photodegradation under simulated sunlight irradiation. Sep Purif Technol 248:116924

Kumar R, Sudhaik A, Khan AAP, Raizada P, Asiri AM, Mohapatra S, Thakur S, Thakur VK, Singh P (2022) Current status on designing of dual Z-scheme photocatalysts for energy and environmental applications. J Ind Eng Chem 106:340–355

Kutuzova A, Dontsova T, Kwapinski W (2021) Application of TiO_2-based photocatalysts to antibiotics degradation: cases of sulfamethoxazole, trimethoprim and ciprofloxacin. Catalysts 11:728

Le AT, Le TDH, Cheong K-Y, Pung S-Y (2022) Immobilization of zinc oxide-based photocatalysts for organic pollutant degradation: a review. J Environ Chem Eng 10:108505

Leong KH, Lim PF, Sim LC, Punia V, Pichiah S (2018) Improved solar light stimulated charge separation of g-C_3N_4 through self-altering acidic treatment. Appl Surf Sci 430:355–361

Li G, Wang B, Zhang J, Wang R, Liu H (2020a) Er-doped g-C_3N_4 for photodegradation of tetracycline and tylosin: high photocatalytic activity and low leaching toxicity. Chem Eng J 391:123500

Li Q, Zhao W, Zhai Z, Ren K, Wang T, Guan H, Shi H (2020b) 2D/2D Bi_2MoO_6/g-C_3N_4 S-scheme heterojunction photocatalyst with enhanced visible-light activity by Au loading. J Mater Sci Technol 56:216–226

Li Y, Xing X, Pei J, Li R, Wen Y, Cui S, Liu T (2020c) Automobile exhaust gas purification material based on physical adsorption of tourmaline powder and visible light catalytic decomposition of g-C_3N_4/$BiVO_4$. Ceram Int 46:12637–12647

Li K, Chen J, Ao Y, Wang P (2021a) Preparation of a ternary g-C_3N_4-CdS/$Bi_4O_5I_2$ composite photocatalysts with two charge transfer pathways for efficient degradation of acetaminophen under visible light irradiation. Sep Purif Technol 259:118177

Li R, Cui X, Bi J, Ji X, Li X, Wang N, Huang Y, Huang X, Hao H (2021b) Urea-induced supramolecular self-assembly strategy to synthesize wrinkled porous carbon nitride nanosheets for highly-efficient visible-light photocatalytic degradation. RSC Adv 11:23459–23470

Liang X, Wang G, Dong X, Wang G, Ma H, Zhang X (2018) Graphitic carbon nitride with carbon vacancies for photocatalytic degradation of bisphenol A. ACS Appl Nano Mater 2:517–524

Liang J, Yang X, Wang Y, He P, Fu H, Zhao Y, Zou Q, An X (2021) A review on g-C_3N_4 incorporated with organics for enhanced photocatalytic water splitting. J Mater Chem A 9:12898–12922

Lin Y, Wu S, Li X, Wu X, Yang C, Zeng G, Peng Y, Zhou Q, Lu L (2018) Microstructure and performance of Z-scheme photocatalyst of silver phosphate modified by MWCNTs and Cr-doped $SrTiO_3$ for malachite green degradation. Appl Catal B-Environ 227:557–570

Liu B, Yang F, Zou Y, Peng Y (2014a) Adsorption of phenol and p-nitrophenol from aqueous solutions on metal-organic frameworks: effect of hydrogen bonding. J Chem Eng Data 59:1476–1482

Liu J, Huang J, Zhou H, Antonietti M (2014b) Uniform graphitic carbon nitride nanorod for efficient photocatalytic hydrogen evolution and sustained photoenzymatic catalysis. ACS Appl Mater Inter 6:8434–8440

Liu X, Pang F, He M, Ge J (2017) Confined reaction inside nanotubes: New approach to mesoporous g-C_3N_4 photocatalysts. Nano Res 10:3638–3647

Liu Q, Shen J, Yu X, Yang X, Liu W, Yang J, Tang H, Xu H, Li H, Li Y, Xu J (2019) Unveiling the origin of boosted photocatalytic hydrogen evolution in simultaneously (S, P, O)-Codoped and exfoliated ultrathin g-C_3N_4 nanosheets. Appl Catal B-Environ 248:84–94

Liu G, Liao M, Zhang Z, Wang H, Chen D, Feng Y (2020) Enhanced photodegradation performance of Rhodamine B with g-C_3N_4 modified by carbon nanotubes. Sep Purif Technol 244:116618

Liu J, Han D, Chen P, Zhai L, Wang Y, Chen W, Mi L, Yang L (2021a) Positive roles of Br in g-C_3N_4/PTCDI-Br heterojunction for photocatalytic degrading chlorophenols. Chem Eng J 418:129492

Liu Z, Huang J, Shao B, Zhong H, Liang Q, He Q, Wu T, Pan Y, Peng Z, Yuan X, Liu Y, Zhao C (2021b) In-situ construction of 2D/1D $Bi_2O_2CO_3$ nanoflake/S-doped g-C_3N_4 hollow tube hierarchical heterostructure with enhanced visible-light photocatalytic activity. Chem Eng J 426:130767

Liu X, Verma G, Chen Z, Hu B, Huang Q, Yang H, Ma S, Wang X (2022) Metal-organic framework nanocrystal-derived hollow porous materials: synthetic strategies and emerging applications. Innovation 3:100281

Lu S, Shen L, Li X, Yu B, Ding J, Gao P, Zhang H (2022a) Advances in the photocatalytic reduction functions of graphitic carbon nitride-based photocatalysts in environmental applications: a review. J Clean Prod 378:13459

Lu Y, Cai Y, Zhang S, Zhuang L, Hu B, Wang S, Chen J, Wang X (2022b) Application of biochar-based photocatalysts for adsorption-(photo)degradation/reduction of environmental contaminants: mechanism, challenges and perspective. Biochar 4:45

Luo YD, Yu SH, Li B, Dong LH, Wang F, Fan MG et al (2016) Synthesis of (Ag, F)-modified anatase TiO_2 nanosheets and their enhanced photocatalytic activity. New J Chem 40:2135–2144

Luo J, Liu Y, Fan C, Tang L, Yang S, Liu M, Wang M, Feng C, Ouyang X, Wang L, Xu L, Wang J, Yan M (2021) Direct Attack and indirect transfer mechanisms dominated by reactive oxygen species for photocatalytic H_2O_2 production on g-C_3N_4 possessing nitrogen vacancies. ACS Catal 11:11440–11450

Luo J, Dai Z, Feng M, Gu M, Xie Y (2022a) Graphitic carbon nitride/ferroferric oxide/reduced graphene oxide nanocomposite as highly active visible light photocatalyst. Nano Res 16:371–376

Luo Y, Han Y, Hua Y, Xue M, Yu S, Zhang L, Yin Z, Li X, Ma X, Wu H, Liu T, Shen Y, Gao B (2022b) Step scheme nickel-aluminium layered double hydroxides/biochar heterostructure photocatalyst for synergistic adsorption and photodegradation of tetracycline. Chemosphere 309:136802

Luo Y, Han Y, Xue M, Xie Y, Yin Z, Xie C, Li X, Zheng Y, Huang J, Zhang Y, Yang Y, Gao B (2022c) Ball-milled bismuth oxybromide/biochar composites with enhanced removal of reactive red owing to the synergy between adsorption and photodegradation. J Environ Manage 308:114652

Luo Y, Wang Y, Hua F, Xue M, Xie X, Xie Y, Yu S, Zhang L, Yin Z, Xie C, Hong Z (2023) Adsorption and photodegradation of reactive red 120 with nickel-iron-layered double hydroxide/biochar composites. J Hazard Mater 443:130300

Ma J, Liang C, Li H, Xu H, Hua Y, Wang C (2021a) A novel composite material based on hydroxylated g-C_3N_4 and oxygen-vacant TiO_2 for improvement of photocatalytic performance. Appl Surf Sci 546:149085

Ma Z, Zhou P, Zhang L, Zhong Y, Sui X, Wang B, Ma Y, Feng X, Xu H, Mao Z (2021b) g-C_3N_4 nanosheets exfoliated by green wet ball milling process for photodegradation of organic pollutants. Chem Phys Lett 766:138335

Ma M, Lin Y, Maheskumar V, Li P, Li J, Wang Z, Zhang M, Jiang Z, Zhang R (2022) A highly efficient (Mo, N) codoped $ZnIn_2S_4$/g-C_3N_4 Z-scheme photocatalyst for the degradation of methylene blue. Appl Surf Sci 585:152607

Majumdar A, Ghosh U, Pal A (2021) Novel 2D/2D g-C_3N_4/Bi_4NbO_8Cl nanocomposite for enhanced photocatalytic degradation of oxytetracycline under visible LED light irradiation. J Colloid Interf Sci 584:320–331

Margolis DJ, Fanelli M, Hoffstad O, Lewis JD (2010) Potential association between the oral tetracycline class of antimicrobials used to treat acne and inflammatory bowel disease. Am J Gastroenterol 105:2610–2616

Mian W, Yubin Z, Guohui D, Chuanyi W (2020) Br-doping of g-C_3N_4 towards enhanced photocatalytic performance in Cr (VI) reduction. Chinese J Catal 41(10):1498–1510

Moradi M, Hasanvandian F, Isari AA, Hayati F, Kakavandi B, Setayesh SR (2021) CuO and ZnO co-anchored on g-C_3N_4 nanosheets as an affordable double Z-scheme nanocomposite for photocatalytic decontamination of amoxicillin. Appl Catal B-Environ 285:119838

Mu R, Ao Y, Wu T, Wang C, Wang P (2020) Synthesis of novel ternary heterogeneous anatase-TiO_2 (B) biphase nanowires/$Bi_4O_5I_2$ composite photocatalysts for the highly efficient degradation of acetaminophen under visible light irradiation. J Hazard Mater 382:121083

Nguyen TKA, Pham T-T, Gendensuren B, Oh E-S, Shin EW (2022) Defect engineering of water-dispersible g-C_3N_4 photocatalysts by chemical oxidative etching of bulk g-C_3N_4 prepared in different calcination atmospheres. J Mater Sci Technol 103:232–243

Niu P, Zhang L, Liu G, Cheng H-M (2012) Graphene-like carbon nitride nanosheets for improved photocatalytic activities. Adv Funct Mater 22:4763–4770

Niu B, Xiao J, Xu Z (2022) Recycling spent $LiCoO_2$ battery as a high-efficient lithium-doped graphitic carbon nitride/Co_3O_4 composite photocatalyst and its synergistic photocatalytic mechanism. Energy Environ Mater

Oliveira CA, Penteado ED, Tomita IN, Santos-Neto AJ, Zaiat M, Silva BFD, Lima Gomes PCF (2019) Removal kinetics of sulfamethazine and its transformation products formed during treatment using a horizontal flow-anaerobic immobilized biomass bioreactor. J Hazard Mater 365:34–43

Ong WJ, Tan LL, Ng YH, Yong ST, Chai SP (2016) Graphitic carbon nitride (g-C_3N_4)-based photocatalysts for artificial photosynthesis and environmental remediation: are we a step closer to achieving sustainability? Chem Rev 116:7159–7329

Paragas LKB, Dien Dang V, Sahu RS, Garcia-Segura S, de Luna MDG, Pimentel JAI, Doong R-A (2021) Enhanced visible-light-driven photocatalytic degradation of acetaminophen over CeO_2/I, K-codoped C_3N_4 heterojunction with tunable properties in simulated water matrix. Sep Purif Technol 272:117567

Phoon BL, Husin JMB, Lee KC, Leo BF, Yang TC, Lai CW, Juan JC (2022) Crystallinity and lattice vacancies of different mesoporous g-C_3N_4 for photodegradation of tetracycline and its cytotoxic implication. Chemosphere 308:136219

Pi Y, Li X, Xia Q, Wu J, Li Y, Xiao J, Li Z (2018) Adsorptive and photocatalytic removal of Persistent Organic Pollutants (POPs) in water by metal-organic frameworks (MOFs). Chem Eng J 337:351–371

Prabavathi S, Saravanakumar K, Mamba G, Muthuraj V (2019) 1D/2D $MnWO_4$ nanorods anchored on g-C_3N_4 nanosheets for enhanced photocatalytic degradation ofloxacin under visible light irradiation. Colloid Surface A 581:123845

Qi H, Shi C, Jiang X, Teng M, Sun Z, Huang Z, Pan D, Liu S, Guo Z (2020) Constructing CeO_2/nitrogen-doped carbon quantum dot/g-C_3N_4 heterojunction photocatalysts for highly efficient visible light photocatalysis. Nanoscale 12:19112–19120

Qin D, Xia Y, Li Q, Yang C, Qin Y, Lv K (2020) One-pot calcination synthesis of $Cd_{0.5}Zn_{0.5}S$/g-C_3N_4 photocatalyst with a step-scheme heterojunction structure. J Mater Sci Technol 56:206–215

Qin K, Zhao Q, Yu H, Xia X, Li J, He S, Wei L, An T (2021) A review of bismuth-based photocatalysts for antibiotic degradation: insight into the photocatalytic degradation performance, pathways and relevant mechanisms. Environ Res 199:111360

Qiu M, Hu B, Chen Z, Yang H, Zhuang L, Wang X (2021) Challenges of organic pollutant photocatalysis by biochar-based catalysts. Biochar 3:117–123

Qu Z, Liu Z, Wu A, Piao C, Li S, Wang J, Song Y (2020) Preparation of a coated Z-scheme and H-type $SrTiO_3$/($BiFeO_3$@ZnS) composite photocatalyst and application in degradation of 2,4-dichlorophenol with simultaneous conversion of Cr(VI). Sep Purif Technol 240:116653

Rabani I, Zafar R, Subalakshmi K, Kim HS, Bathula C, Seo YS (2021) A facile mechanochemical preparation of Co_3O_4@g-C_3N_4 for application in supercapacitors and degradation of pollutants in water. J Hazard Mater 407:124360

Raja A, Rajasekaran P, Selvakumar K, Arunpandian M, Kaviyarasu K, Asath Bahadur S, Swaminathan M (2020) Visible active reduced graphene oxide-$BiVO_4$-ZnO ternary photocatalyst for efficient removal of ciprofloxacin. Sep Purif Technol 233:115996

Rauf MA, Ashraf SS (2009) Fundamental principles and application of heterogeneous photocatalytic degradation of dyes in solution. Chem Eng J 151:10–18

Raval NP, Shah PU, Shah NK (2016) Adsorptive amputation of hazardous azo dye Congo red from wastewater: a critical review. Environ Sci Pollut Res Int 23:14810–14853

Raziq F, Hayat A, Humayun M, Baburao Mane SK, Faheem MB, Ali A, Zhao Y, Han S, Cai C, Li W, Qi D-C, Yi J, Yu X, Breese MBH, Hassan F, Ali F, Mavlonov A, Dhanabalan K, Xiang X, Zu X, Li S, Qiao L (2020) Photocatalytic solar fuel production and environmental remediation through experimental and DFT based research on CdSe-QDs-coupled P-doped-g-C_3N_4 composites. Appl Catal B-Environ 270:118867

Ren K, Lv M, Xie Q, Zhang C, Shi H (2022) Dual BN quantum dot/Ag co-catalysts synergistically promote electron-hole separation on g-C_3N_4 nanosheets for efficient antibiotics oxidation and Cr (VI) reduction. Carbon 186:355–366

Roca Jalil ME, Baschini M, Sapag K (2015) Influence of pH and antibiotic solubility on the removal of ciprofloxacin from aqueous media using montmorillonite. Appl Clay Sci 114:69–76

Roselin LS, Patel N, Khayyat SA (2019) Codoped g-C_3N_4 nanosheet for degradation of organic pollutants from oily wastewater. Appl Surf Sci 494:952–958

Saravanakumar K, Park CM (2021) Rational design of a novel $LaFeO_3$/g-C_3N_4/$BiFeO_3$ double Z-scheme structure: photocatalytic performance for antibiotic degradation and mechanistic insight. Chem Eng J 423:130076

Seng RX, Tan LL, Lee WPC, Ong WJ, Chai SP (2020) Nitrogen-doped carbon quantum dots-decorated 2D graphitic carbon nitride as a promising photocatalyst for environmental remediation: a study on the importance of hybridization approach. J Environ Manage 255:109936

Sepehrmansourie H, Alamgholiloo H, Noroozi Pesyan N, Zolfigol MA (2023) A MOF-on-MOF strategy to construct double Z-scheme heterojunction for high-performance photocatalytic degradation. Appl Catal B-Environ 321:122082

Shen H, Li M, Guo W, Li G, Xu C (2020) P, K co-doped porous g-C_3N_4 with enhanced photocatalytic activity synthesized in vapor and self-producing NH_3 atmosphere. Appl Surf Sci 507:145086

Shurbaji S, Huong PT, Altahtamouni TM (2021) Review on the visible light photocatalysis for the decomposition of ciprofloxacin, norfloxacin, tetracyclines, and sulfonamides antibiotics in wastewater. Catalysts 11:437

Song Y, Tian J, Gao S, Shao P, Qi J, Cui F (2017) Photodegradation of sulfonamides by g-C_3N_4 under visible light irradiation: effectiveness, mechanism and pathways. Appl Catal B-Environ 210:88–96

Song B, Zeng Z, Zeng G, Gong J, Xiao R, Ye S, Chen M, Lai C, Xu P, Tang X (2019) Powerful combination of g-C_3N_4 and LDHs for enhanced photocatalytic performance: a review of strategy, synthesis, and applications. Adv Colloid Interfac 272:101999

Sudhaik A, Raizada P, Shandilya P, Jeong D-Y, Lim J-H, Singh P (2018) Review on fabrication of graphitic carbon nitride based efficient nanocomposites for photodegradation of aqueous phase organic pollutants. J Int Eng Chem 67:28–51

Sun L, Zhou Y, Li X, Li J, Shen D, Yin S, Wang H, Huo P, Yan Y (2020) Thermo-responsive functionalized PNIPAM@Ag/Ag_3PO_4/CN-heterostructure photocatalyst with switchable photocatalytic activity. Chinese J Catal 41:1573–1588

Sun D, Jia L, Wang C, Liu H, Chen R (2021a) Preparation of the additive-modified α-Fe_2O_3/g-C_3N_4 Z-scheme composites with improved visible-light photocatalytic activity. J Env Chem Eng 9:106274

Sun S, Li C, Sun Z, Wang J, Wang X, Ding H (2021b) In-situ design of efficient hydroxylated SiO_2/g-C_3N_4 composite photocatalyst: synergistic effect of compounding and surface hydroxylation. Chem Eng J 416:129107

Sun L, Feng Y, Ma K, Jiang X, Gao Z, Wang J, Jiang N, Liu X (2022) Synergistic effect of single-atom Ag and hierarchical tremella-like g-C_3N_4: electronic structure regulation and multi-channel carriers transport for boosting photocatalytic performance. Appl Catal B-Environ 306:121106

Taizo S, Sakiko T, Kazuhide K, Tsutomu H, Yoshiyuki T, Nobuaki N et al (2013) Activation of graphitic carbon nitride (g-C_3N_4) by alkaline hydrothermal treatment for photocatalytic NO oxidation in gas phase. J Mater Chem A 1(21):6489–6496

Tan J, Tian N, Li Z, Li J, Yao X, Vakili M, Lu Y, Zhang T (2021) Intrinsic defect engineering in graphitic carbon nitride for photocatalytic environmental purification: a review to fill existing knowledge gaps. Chem Eng J 421:127729

Tang C, Cheng M, Lai C, Li L, Yang X, Du L, Zhang G, Wang G, Yang L (2023) Recent progress in the applications of non-metal modified graphitic carbon nitride in photocatalysis. Coordin Chem Rev 474:214846

Tian J, Chen Z, Deng X, Sun Q, Sun Z, Li W (2018) Improving visible light driving degradation of norfloxacin over core-shell hierarchical BiOCl

microspherical photocatalyst by synergistic effect of oxygen vacancy and nanostructure. Appl Surf Sci 453:373–382
Uddin A, Rauf A, Wu T, Khan R, Yu Y, Tan L, Jiang F, Chen H (2021) In_2O_3/oxygen doped g-C_3N_4 towards photocatalytic BPA degradation: balance of oxygen between metal oxides and doped g-C_3N_4. J Colloid Interf Sci 602:261–273
Velmurugan S, Balu S, Palanisamy S, Yang TCK, Velusamy V, Chen S-W, El-Shafey E-SI (2020) Synthesis of novel and environmental sustainable AgI-Ag_2S nanospheres impregnated g-C_3N_4 photocatalyst for efficient degradation of aqueous pollutants. Appl Surf Sci 500:143911
Wang J, Xia Y, Zhao H, Wang G, Xiang L, Xu J, Komarneni S (2017) Oxygen defects-mediated Z-scheme charge separation in g-C_3N_4/ZnO photocatalysts for enhanced visible-light degradation of 4-chlorophenol and hydrogen evolution. Appl Catal B-Environ 206:406–416
Wang Q, Wang P, Xu P, Li Y, Duan J, Zhang G, Hu L, Wang X, Zhang W (2020) Visible-light-driven photo-Fenton reactions using $Zn_{1-1.5}FeS/_g$-C_3N_4 photocatalyst: degradation kinetics and mechanisms analysis. Appl Catal B-Environ 266:118653
Wang G, Zhao Y, Ma H, Zhang C, Dong X, Zhang X (2021a) Enhanced peroxymonosulfate activation on dual active sites of N vacancy modified g-C_3N_4 under visible-light assistance and its selective removal of organic pollutants. Sci Total Environ 756:144139
Wang J, Wang G, Cheng B, Yu J, Fan J (2021b) Sulfur-doped g-C_3N_4/TiO_2 S-scheme heterojunction photocatalyst for Congo Red photodegradation. Chinese J Catal 42:56–68
Wang X, Chen G, Wang H, Wu Y, Wei X, Wen J, Hu L, Gu W, Zhu C (2021c) Imide modification coupling with NH_2-MIL-53(Fe) boosts the photocatalytic performance of graphitic carbon nitride for efficient water remediation. J Catal 399:192–200
Wang X, Xu G, Tu Y, Wu D, Li A, Xie X (2021d) BiOBr/PBCD-B-D dual-function catalyst with oxygen vacancies for Acid Orange 7 removal: evaluation of adsorption-photocatalysis performance and synergy mechanism. Chem Eng J 411:128456
Wang Y, Li X, Lei W, Zhu B, Yang J (2021e) Novel carbon quantum dot modified g-C_3N_4 nanotubes on carbon cloth for efficient degradation of ciprofloxacin. Appl Surf Sci 559:149967
Wei K, Faraj Y, Yao G, Xie R, Lai B (2021) Strategies for improving perovskite photocatalysts reactivity for organic pollutants degradation: a review on recent progress. Chem Eng J 414:128783
Wen J, Xie J, Chen X, Li X (2017) A review on g-C_3N_4-based photocatalysts. Appl Surf Sci 391:72–123
Wu M, Ding T, Wang Y, Zhao W, Xian H, Tian Y, Zhang T, Li X (2020) Rational construction of plasmon Au assisted ferroelectric-$BaTiO_3$/Au/g-C_3N_4 Z-scheme system for efficient photocatalysis. Catal Today 355:311–318
Wu Y, Zhao X, Huang S, Li Y, Zhang X, Zeng G, Niu L, Ling Y, Zhang Y (2021) Facile construction of 2D g-C_3N_4 supported nanoflower-like $NaBiO_3$ with direct Z-scheme heterojunctions and insight into its photocatalytic degradation of tetracycline. J Hazard Mater 414:125547
Xing J, Wang N, Li X, Wang J, Taiwaikuli M, Huang X, Wang T, Zhou L, Hao H (2022) Synthesis and modifications of g-C_3N_4-based materials and their applications in wastewater pollutants removal. J Environ Chem Eng 10:108782
Xu Q, Zhang L, Yu J, Wageh S, Al-Ghamdi AA, Jaroniec M (2018) Direct Z-scheme photocatalysts: principles, synthesis, and applications. Mater Today 21:1042–1063
Xu Y, Ge F, Chen Z, Huang S, Wei W, Xie M, Xu H, Li H (2019) One-step synthesis of Fe-doped surface-alkalinized g-C_3N_4 and their improved visible-light photocatalytic performance. Appl Surf Sci 469:739–746
Xu F, Mo Z, Yan J, Fu J, Song Y, El-Alami W, Wu X, Li H, Xu H (2020a) Nitrogen-rich graphitic carbon nitride nanotubes for photocatalytic hydrogen evolution with simultaneous contaminant degradation. J Colloid Interf Sci 560:555–564
Xu W, Lai S, Pillai SC, Chu W, Hu Y, Jiang X, Fu M, Wu X, Li F, Wang H (2020b) Visible light photocatalytic degradation of tetracycline with porous Ag/graphite carbon nitride plasmonic composite: degradation pathways and mechanism. J Colloid Interf Sci 574:110–121
Xu L, Li L, Yu L, Yu JC (2022) Efficient generation of singlet oxygen on modified g-C_3N_4 photocatalyst for preferential oxidation of targeted organic pollutants. Chem Eng J 431:134241
Yang Y, Bian Z (2021) Oxygen doping through oxidation causes the main active substance in g-C_3N_4 photocatalysis to change from holes to singlet oxygen. Sci Total Environ 753:141908
Yang D, Wang W, An K, Chen Y, Zhao Z, Gao Y, Jiang Z (2021) Bioinspired construction of carbonized poly(tannic acid)/g-C_3N_4 nanorod photocatalysts for organics degradation. Appl Surf Sci 562:150256
Ye S, Zhou X, Xu Y, Lai W, Yan K, Huang L, Ling J, Zheng L (2019) Photocatalytic performance of multi-walled carbon nanotube/$BiVO_4$ synthesized by electro-spinning process and its degradation mechanisms on oxytetracycline. Chem Eng J 373:880–890
Yi F, Gan H, Jin H, Zhao W, Zhang K, Jin H, Zhang H, Qian Y, Ma J (2020) Sulfur- and chlorine-co-doped g-C_3N_4 nanosheets with enhanced active species generation for boosting visible-light photodegradation activity. Sep Purif Technol 233:115997
Yuan X, Qu S, Huang X, Xue X, Yuan C, Wang S, Wei L, Cai P (2021a) Design of core-shelled g-C_3N_4@ZIF-8 photocatalyst with enhanced tetracycline adsorption for boosting photocatalytic degradation. Chem Eng J 416:129148
Yuan Y, Guo R-t, Hong L-f, Ji X-y, Lin Z-d, Li Z-s, Pan W-g (2021b) A review of metal oxide-based Z-scheme heterojunction photocatalysts: actualities and developments. Mater Today Energy 21:100829
Zhang D, Qiu R, Song L, Eric B, Mo Y, Huang X (2009) Role of oxygen active species in the photocatalytic degradation of phenol using polymer sensitized TiO_2 under visible light irradiation. J Hazard Mater 163:843–847
Zhang S, Gu P, Ma R, Luo C, Wen T, Zhao G, Cheng W, Wang X (2019) Recent developments in fabrication and structure regulation of visible-light-driven g-C_3N_4-based photocatalysts towards water purification: a critical review. Catal Today 335:65–77
Zhang C, Zhou Y, Wang W, Yang Y, Zhou C, Wang L, Lei L, He D, Luo H, Huang D (2020a) Formation of Mo_2C/hollow tubular g-C_3N_4 hybrids with favorable charge transfer channels for excellent visible-light-photocatalytic performance. Appl Surf Sci 527:146757
Zhang X, Wang J, Dong XX, Lv YK (2020b) Functionalized metal-organic frameworks for photocatalytic degradation of organic pollutants in environment. Chemosphere 242:125144
Zhang Q, Peng Y, Lin Y, Wu S, Yu X, Yang C (2021a) Bisphenol S-doped g-C_3N_4 nanosheets modified by boron nitride quantum dots as efficient visible-light-driven photocatalysts for degradation of sulfamethazine. Chem Eng J 405:126661
Zhang S, Zhang Z, Li B, Dai W, Si Y, Yang L, Luo S (2021b) Hierarchical Ag_3PO_4@$ZnIn_2S_4$ nanoscoparium: an innovative Z-scheme photocatalyst for highly efficient and predictable tetracycline degradation. J Colloid Interf Sci 586:708–718
Zhang T, Maihemllti M, Okitsu K, Talifur D, Tursun Y, Abulizi A (2021c) In situ self-assembled S-scheme BiOBr/pCN hybrid with enhanced photocatalytic activity for organic pollutant degradation and CO_2 reduction. Appl Surf Sci 556:149828
Zhang W, Bian Z, Xin X, Wang L, Geng X, Wang H (2021d) Comparison of visible light driven H_2O_2 and peroxymonosulfate degradation of norfloxacin using Co/g-C_3N_4. Chemosphere 262:127955
Zhang X, Wang X, Meng J, Liu Y, Ren M, Guo Y, Yang Y (2021e) Robust Z-scheme g-C_3N_4/WO_3 heterojunction photocatalysts with morphology control of WO_3 for efficient degradation of phenolic pollutants. Sep Purif Technol 255:117693
Zhang S, Liu Y, Ma R, Jia D, Wen T, Ai Y, Zhao G, Fang F, Hu B, Wang X (2022a) Molybdenum (VI)-oxo clusters incorporation activates g-C_3N_4 with simultaneously regulating charge transfer and reaction centers for boosting photocatalytic performance. Adv Funct Mater 32:2204175
Zhang Y, Liu H, Gao F, Tan X, Cai Y, Hu B, Huang Q, Fang M, Wang X (2022b) Application of MOFs and COFs for photocatalysis in CO_2 reduction, H_2 generation, and environmental treatment. EnergyChem 4:100078
Zhao H, Yu H, Quan X, Chen S, Zhao H, Wang H (2013) Atomic single layer graphitic-C_3N_4: fabrication and its high photocatalytic performance under visible light irradiation. RSC Adv 4(2):624–628
Zhao C, Ran F, Dai L, Li C, Zheng C, Si C (2021a) Cellulose-assisted construction of high surface area Z-scheme C-doped g-C_3N_4/WO_3 for improved tetracycline degradation. Carbohyd Polym 255:117343
Zhao G, Ding J, Zhou F, Chen X, Wei L, Gao Q, Wang K, Zhao Q (2021b) Construction of a visible-light-driven magnetic dual Z-scheme $BiVO_4$/g-C_3N_4/$NiFe_2O_4$ photocatalyst for effective removal of ofloxacin: mechanisms and degradation pathway. Chem Eng J 405:126704

Zhao W, Li J, She T, Ma S, Cheng Z, Wang G, Zhao P, Wei W, Xia D, Leung DYC (2021c) Study on the photocatalysis mechanism of the Z-scheme cobalt oxide nanocubes/carbon nitride nanosheets heterojunction photocatalyst with high photocatalytic performances. J Hazard Mater 402:123839

Zhao W, She T, Zhang J, Wang G, Zhang S, Wei W, Yang G, Zhang L, Xia D, Cheng Z, Huang H, Leung DYC (2021d) A novel Z-scheme CeO_2/g-C_3N_4 heterojunction photocatalyst for degradation of Bisphenol A and hydrogen evolution and insight of the photocatalysis mechanism. J Mater Sci Technol 85:18–29

Zheng Y, Lin LH, Wang B, Wang XC (2015) Graphitic carbon nitride polymers toward sustainable photoredox catalysis. Angew Chem Int Edit 54:12868–12884

Zheng X, Zhang Q, Chen T, Wu Y, Hao J, Tan C, Chen P, Wang F, Liu H, Lv W, Liu G (2020) A novel synthetic carbon and oxygen doped stalactite-like g-C_3N_4 for broad-spectrum-driven indometacin degradation. J Hazard Mater 386:121961

Zhou L, Zhang W, Chen L, Deng H (2017) Z-scheme mechanism of photogenerated carriers for hybrid photocatalyst Ag_3PO_4/g-C_3N_4 in degradation of sulfamethoxazole. J Colloid Interf Sci 487:410–417

Zhou S, Hou M, Sun Y, Zhao W, Wang H, Guo Q, Yu X, Ma X, Zhao J (2021) Ultra-high-performance visible-light photodegradation enabled by direct Z-scheme AgI/(Na, F)–C_3N_4 composites. Compos Part B-Eng 224:109200

Zhu D, Zhou Q (2021) Nitrogen doped g-C_3N_4 with the extremely narrow band gap for excellent photocatalytic activities under visible light. Appl Catal B-Environ 281:119474

Zhu Z, Ma C, Yu K, Lu Z, Liu Z, Huo P, Tang X, Yan Y (2020) Synthesis Ce-doped biomass carbon-based g-C_3N_4 via plant growing guide and temperature-programmed technique for degrading 2-Mercaptobenzothiazole. Appl Catal B-Environ 268:118432

Publisher's Note

Springer Nature remains neutral with regard to jurisdictional claims in published maps and institutional affiliations.